universe

MDPI

Review

RR Lyrae Stars and Anomalous Cepheids as Population Tracers in Local Group Galaxies

Matteo Monelli [1,2,*] and Giuliana Fiorentino [3]

[1] IAC Instituto de Astrofísica de Canarias, Calle Vía Láctea sn, E-38201 La Laguna, Spain
[2] Departamento de Astrofísica, Universidad de La Laguna, E-38206 La Laguna, Spain
[3] Osservatorio Astronomico di Roma, Via Frascati 33, 00078 Monte Porzio Catone, Italy; giuliana.fiorentino@inaf.it
* Correspondence: monelli@iac.es

Abstract: We discuss the use and importance of pulsating variable stars as population tracers in Local Group galaxies. Among bright variable crossing the classical instability strip, we mostly focus on RR Lyrae stars and Anomalous Cepheids. We discuss their pulsational properties and how it is possible to use them to constrain the evolution and star formation history of the host galaxy. We discuss RR Lyrae stars as tracers of the old population, and how they can be used to trace the accretion history of large galaxies such as the Milky Way and M31, and also the early chemical evolution. Moreover, we show that the frequency of Anomalous Cepheids follows different relations, and therefore trace the intermediate-age star formation. Finally, we discuss the different methods to derive distances and the impact of the Gaia mission.

Keywords: variable stars; RR Lyrae stars; Anomalous Cepheids; Local Group; dwarf galaxies; resolved stellar populations

Citation: Monelli, M.; Fiorentino, G. RR Lyrae Stars and Anomalous Cepheids as Population Tracers in Local Group Galaxies. *Universe* **2022**, *8*, 191. https://doi.org/10.3390/universe8030191

Academic Editor: Sylvia Ekström

Received: 1 December 2021
Accepted: 10 March 2022
Published: 19 March 2022

1. Introduction

Pulsating variable stars are at the cornerstone of many astrophysical fields: stellar pulsation, stellar evolution, stellar atmospheres, dynamical phenomena, stellar populations, chemical evolution, distance scale (Bono et al. [1], Marconi et al. [2], Kolenberg et al. [3], Benkő and Szabó [4], Feast and Walker [5], Riess et al. [6]). As such, they are powerful instruments to understand the evolution of the host galaxy, as they provide direct insights on the age and metallicity distribution of their parent population (De Somma et al. [7], Martínez-Vázquez et al. [8]).

Pulsating variable stars are therefore essential beacons of the so-called "Galactic Archaeology", which uses resolved nearby galaxies in the Local Group (LG) to answer fundamental questions about galaxy formation and evolution (Tolstoy et al. [9]). According to the Lambda cold dark matter model, dwarf galaxies are relatively simple systems and the first ones to form. They participate in the build-up of larger galaxies and thus they are ideal targets to unravel the physics governing the formation and early evolution of galactic structures and essential probes of the physical ingredients included in current galaxy formation and evolution models (Dekel and Silk [10], Sawala et al. [11], Mayer et al. [12]). In this context, LG galaxies offer a fantastic playground for detailed study of the mechanisms driving galaxy evolution, because of the large variety of dwarf galaxies with different morphological and evolutionary properties, and living in different environments. Moreover, they can be resolved into individual stars, for which ages and metallicities can be determined with the help of stellar evolution and stellar atmospheres theory, together with the use of different complementary observational techniques (Gallart et al. [13]).

Using pulsating variable stars in LG galaxies add extra observables to colour-magnitude diagrams (CMDs), spectroscopy and astrometric information such those provided by the

Gaia mission. This complementarity is enriched by the variety of the variability phenomenology. Pulsating variable stars include many different groups and families, with different observational properties (period, amplitude, pulsation mode) and populating different regions of the CMD. In this paper we mainly focus on RR Lyrae stars (RRLs) and Anomalous Cepheids (ACs), but we also discuss other bright pulsating variable stars observed in LG dwarf galaxies with distance $\leq$ 2 Mpc, that is Type II (TIIC) and short-period Classical Cepheids (CCs). The property common to all these objects is the fact that they are crossing the classical Instability Strip (IS) during, or just after, their central Helium burning evolutionary phase (Marconi et al. [2], Bono et al. [14,15]).

We are now facing a golden age for variable star studies. In the last two decades, many wide-field or full sky surveys has provided large data bases of photometric optical and near infrared (NIR) data of the Milky Way (MW) and LG galaxies (e.g., Optical Gravitational Lensing Experiment-OGLE: Udalski et al. [16]; QUEST: Zinn et al. [17]; Northern Sky Variability Survey-NSVS: Woźniak et al. [18]; All Sky Automates Survey-ASAS: Szczygieł et al. [19]; Catalina Sky Survey-CSS: Drake et al. [20]; Vista Magellanic Clouds-VMC: Cioni et al. [21]; VISTA Variables in the Via Lactea-VVV: Minniti et al. [22]; Wide-field Infrared Survey Explorer-WISE: Wright et al. [23]; Panoramic Survey Telescope and Rapid Response System- Pan-STARRS: Chambers et al. [24]). At present, the European Space Agency mission Gaia has provided parallaxes, hence distances, of unprecedented accuracy which are pushing a huge step forward in the establishment of the cosmic distance scale. The next Gaia DR3, expected for June 2022, will release identification and light curves for $\sim$13 million variable stars, which will set a fundamental benchmark for future investigations. Moreover, ongoing large surveys exploring the time domain such as the ZTF (Masci et al. [25], Bellm et al. [26]) are not only providing complementary multiband information, but are the training ground for the next-to-come huge projects such as the Rubin-LSST (Ivezić et al. [27]), expected to start at the beginning of 2023. Finally, large field-of-view spectroscopic facilities such as WEAVE, which will see its first light in 2022 at the William Herschel Telescope, will also provide high resolution chemical abundances for a large number of field variable stars.

2. Observational Properties

Table 1 lists galaxies in and next to the LG, within 2 Mpc, with known variable stars[1]. The table presents name, coordinates, the subgroup of each galaxy, and the number of RRab, RRc, Anomalous, Classic, and Type II Cepheids. The last two columns show the photometric system in which the variable stars data have been collected, and the relevant references. To summarize the observational properties of bright pulsating variable stars in the IS, we show the OGLE sample of LMC variables in both the reddened CMD (see Figure 1) and in the Wesenheit diagram [$I - 1.54(V - I)$, see Figure 2], which is by construction reddening-free[2]. See the caption for the details about the colour code adopted to display the different classes and pulsation modes. The data are taken from the OGLE III project, in particular RRLs are presented in Soszyński et al. [28], CCs in Soszyński et al. [29] and finally TIICs and ACs are discussed in Soszyński et al. [30]. In the CMD the considered variable stars partially overlap, making the separation among the different classes difficult. Since also the period ranges partially overlap, the Wesenheit diagram seems to be the best tool to properly classify different types of variables according to their magnitude/colour/period distribution. This is shown in Figure 3, which shows the period distribution of the four different types of pulsators, for the same stars as in Figure 1.

Table 1. List of nearby galaxies with known variable stars. Columns present name, right ascension, declination, sub-group within the Local Group, number of RRab, RRc, ACs, CCs, and TIICs, passband of the available photometry (the asterisks marks data collected with the HST and published after calibrating the photometry to the Johnson system), references. The double asterisks mark the cases in which the classification of AC and short period CCs is subject to uncertainty. Note the case of Pegasus III and Pisces 2, which hosts one variable star with uncertain classification (RRL or AC star).

Galaxy	R.A.	Dec.	Group	N_{RRab}	N_{RRcd}	N_{AC}	N_{CC}	N_{TIIC}	Photometry	Reference
ESO410-G005	00:15:31.6	–32:10:48.0	Scl	225	44	9 **	13 **	0 **	$VI*$	Yang et al. [31]
And XIX	00:19:32.1	+35:02:37.0	M31	31	8	8	0	0	BV	Cusano et al. [32]
Cetus	00:26:11.0	–11:02:40.0	isol	506	124	8	0	0	$BVI, F475W, F814W$	Bernard et al. [33], Monelli et al. [34]
ESO294-G010	00:26:33.4	–41:51:19.0	Scl	219	13	3 **	16 **	0 **	$VI*$	Yang et al. [31]
And XXV	00:30:08.9	+46:51:07.0	M31	46	11	3	0	0	BV	Cusano et al. [35]
NGC 147	00:33:12.1	+48:30:32.0	M31	118	58	2	0	0	$F606W, F555W$	Monelli et al. [36]
And III	00:35:33.8	+36:29:52.0	M31	84	15	4	0	0	$F475W, F814W$	Martínez-Vázquez et al. [37]
And XXVII	00:37:27.1	+45:23:13.0	M31	58	31	1	0	0	BV	Cusano et al. [38]
NGC 185	00:38:58.0	+48:20:15.0	M31	544	272	3	0	0	$F606W, F555W$	Monelli et al. [36]
NGC 205	00:40:22.1	+41:41:07.0	M31	30	0	7	0	0	g	Saha et al. [39]
M 32	00:42:41.8	+40:51:55.0	M31	375	134	4	0	0	$VI*$	Fiorentino et al. [40], Sarajedini et al. [41]
And I	00:45:39.8	+38:02:28.0	M31	229	48	0	0	0	$F475W, F814W$	Martínez-Vázquez et al. [37]
And XI	00:46:20.0	+33:48:05.0	M31	12	5	0	0	0	$VI*$	Yang and Sarajedini [42]
And XIII	00:51:51.0	+33:00:16.0	M31	8	1	0	0	0	$VI*$	Yang and Sarajedini [42]
SMC	00:52:44.8	–72:49:43.0	MW	4961	1407	4915	109	53	VI	Soszyński et al. [43–45]
And XVI	00:59:29.8	+32:22:36.0	M31	3	5	0	0	0	$F475W, F814W$	Martínez-Vázquez et al. [37], Monelli et al. [46]
Sculptor	01:00:09.4	–33:42:33.0	MW	289	247	4	0	0	BVI	Martínez-Vázquez et al. [47]
IC 1613	01:04:47.8	+02:07:04.0	isol	61	29	0	160	0	$F475W, F814W$	Bernard et al. [33], Tammann et al. [48]
And XV	01:14:18.7	+38:07:03.0	M31	80	24	4	0	0	$F475W, F814W$	Martínez-Vázquez et al. [37]
And II	01:16:29.8	+33:25:09.0	M31	187	48	4	0	0	$F475W, F814W$	Martínez-Vázquez et al. [37]
Triangulum	01:33:50.9	+30:39:37.0	M31	85	14	0	?	0	$VI*$	Tanakul et al. [49]
Phoenix	01:51:06.3	–44:26:41.0	isol	54	24	19 **	0	0	$VI*$	Gallart et al. [50], Ordoñez et al. [51]
Segue 2	02:19:16.0	+20:10:31.0	MW	1	0	0	0	0	BV	Boettcher et al. [52]
Eridanus 3	02:22:45.5	–52:17:01.0	MW	0	1	0	0	0	G, G_{BP}, G_{RP}	Vivas et al. [53]
Fornax	02:39:59.3	–34:26:57.0	MW	1493	493	0	5	2	BVI	Braga et al. in prep.
Eridanus 2	03:44:21.1	–43:32:00.0	MW	44	23	2	0	0	$gri, F475W, F814W$	Martínez-Vázquez et al. [54]
Reticulum 3	03:45:26.4	–60:27:00.0	MW	1	0	0	0	0	G, G_{BP}, G_{RP}	Vivas et al. [53]
LMC	05:23:34.5	–69:45:22.0	MW	27620	11461	4628	141	285	VI	Soszyński et al. [43,44,45]
Carina	06:41:36.7	–50:57:58.0	MW	71	21	20	0	0	$UBVI$	Coppola et al. [55]
Carina 2	07:36:25.6	–57:59:57.0	MW	1	1	0	0	0	G, G_{BP}, G_{RP}	Vivas et al. [53]
Ursa Major 2	08:51:30.0	+63:07:48.0	MW	2	2	0	0	0	G, G_{BP}, G_{RP}	Vivas et al. [53]
Hydra 1	08:55:36.0	+03:36:00.0	MW	4	0	0	0	0	G, G_{BP}, G_{RP}	Vivas et al. [53]
UGC4879-VV124	09:16:02.2	+52:50:24.0	isol	532	146	10	78	1	$F475W, F814W$	Neeley et al. [56]
Leo T	09:34:53.4	+17:03:05.0	MW	4	1	17	0	0	$F475W, F606W, F814W$	Surot et al. in prep.
Antlia 2	09:35:32.8	–36:46:02.3	MW	193	104	8	0	0	r, i	Vivas et al. [57]
Leo A	09:59:26.5	+30:44:47.0	isol	7	3	0 **	156 **	0	$F475W, F814W$	Bernard et al. [58]
Segue 1	10:07:04.0	+16:04:55.0	MW	1	0	0	0	0	gi	Simon et al. [59]
Leo 1	10:08:28.1	+12:18:23.0	MW	136	38	55 **	0 **	0	$UBVRI$	Stetson et al. [60]
Sextans	10:13:03.0	–01:36:53.0	MW	26	10	9	0	0	BV, BVI, gr	Mateo et al. [61], Amigo et al. [62], Vivas et al. [63]
Leo P	10:21:45.1	+18:05:17.0	isol	9	1	0	0	0	$F475W, F814W$	McQuinn et al. [64]
Ursa Major 1	10:34:52.8	+51:55:12.0	MW	6	0	0	0	0	G, G_{BP}, G_{RP}	Vivas et al. [53]
Leo 2	11:13:28.8	+22:09:06.0	MW	106	34	4	0	0	BV	Siegel and Majewski [65]
Leo 5	11:31:09.6	+02:13:12.0	MW	3	0	0	0	0	gr	Medina et al. [66]
Leo 4	11:32:57.0	–00:32:00.0	MW	3	0	0	0	0	BV	Moretti et al. [67]
Crater 2	11:49:14.4	–18:24:47.0	MW	84	15	7	0	0	BV, BVI, gri	Joo et al. [68], Monelli et al. [69], Vivas et al. [70]
Hydra 2	12:21:42.1	–31:59:07.0	MW	1	0	0	0	0	gri	Vivas et al. [71]
Coma Berenices	12:26:59.0	+23:54:15.0	MW	2	0	0	0	0	G, G_{BP}, G_{RP}	Vivas et al. [53]
Centaurus 1	12:38:20.4	–40:54:07.2	MW	1	2	0	0	0	gi	Martínez-Vázquez et al. [72]
Canes Venatici 1	13:28:03.5	+33:33:21.0	MW	18	5	3	0	0	BV	Kuehn et al. [73]
Bootes 3	13:57:12.0	+26:48:00.0	MW	4	3	0	0	0	G, G_{BP}, G_{RP}	Vivas et al. [53]
Bootes 2	13:58:00.0	+12:51:00.0	MW	1	0	0	0	0	G, G_{BP}, G_{RP}	Vivas et al. [53]
Bootes 1	14:00:06.0	+14:30:00.0	MW	1	2	0	0	0	G, G_{BP}, G_{RP}	Vivas et al. [53]
Ursa Minor	15:09:08.5	+67:13:21.0	MW	47	35	7	0	0	BV	Nemec et al. [74]
KKR 25	16:13:48.0	+54:22:16.0	isol	39	7	25	0	0	$F475W, F814W$	Neeley et al. [56]
Hercules	16:31:02.0	+12:47:30.0	MW	6	3	1	0	0	B	Musella et al. [75]
Draco	17:20:12.4	+57:54:55.0	MW	211	56	9	0	0	VI	Kinemuchi et al. [76]
Sagittarius dSph	18:55:19.5	–30:32:43.0	MW	1636	409	0	0	174	VI	Soszyński et al. [77], Hamanowicz et al. [78]
NGC 6822	19:44:56.6	–14:47:21.0	isol	24	2	15	30	0	BV	Baldacci et al. [79]
Sagittarius 2	19:52:40.5	–22:04:05.0	MW	2	3	0	0	0	G, G_{BP}, G_{RP}	Vivas et al. [53]
Grus 2	22:04:04.8	–46:26:24.0	MW	0	1	0	0	0	gri	Martínez-Vázquez et al. [80]
Pegasus 3	22:24:22.6	+05:25:12.0	MW	1 *	0	1 *	0	0	BV	Garofalo et al. [81]
And XXVIII	22:32:41.2	+31:12:58.0	M31	35	34	3	0	0	$F475W, F814W$	Martínez-Vázquez et al. [37]
Tucana	22:41:49.6	–64:25:10.0	isol	216	142	7	0	0	$F475W, F814W$	Bernard et al. [82]
Tucana 2	22:51:55.1	–58:34:08.0	MW	1	2	0	0	0	G, G_{BP}, G_{RP}	Vivas et al. [53]
Grus 1	22:56:42.4	–50:09:48.0	MW	2	0	0	0	0	gri	Martínez-Vázquez et al. [80]
Pisces 2	22:58:31.0	+05:57:09.0	MW	1 *	0	1 *	0	0	BV	Garofalo et al. [81]
And VII	23:26:31.7	+50:40:33.0	M31	336	187	7	0	0	$F435W, F555W$	Monelli et al. [36]
Phoenix 2	23:39:59.4	–54:24:22.0	MW	1	0	0	0	0	G, G_{BP}, G_{RP}	Vivas et al. [53]
And VI	23:51:46.3	+24:34:57.0	M31	91	20	6	0	0	$BV*$	Pritzl et al. [83]
And XXI	23:54:47.7	+42:28:15.0	M31	37	4	9	0	0	BV	Cusano et al. [84]
Tucana 3	23:56:36.0	–59:36:00.0	MW	5	1	0	0	0	G, G_{BP}, G_{RP}	Vivas et al. [53]

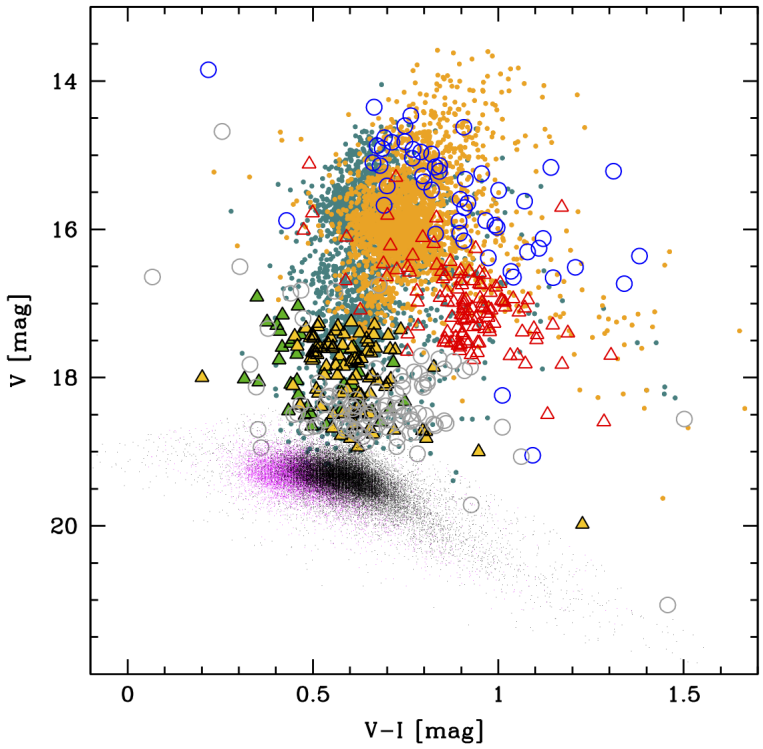

Figure 1. I, V-I Colour magnitude distribution of RRLs, TIICs, ACs and CCs in the LMC. Reddened apparent magnitude are considered. Small points show the location of RRab (black) and RRc (pink) stars. Yellow and green filled triangles are used for fundamental and first overtone ACs, respectively. Similarly, orange and teal filled small circles show fundamental and first overtone CCs. Large open symbols are used for TIICs: BL Her (grey circles), W Vir (red triangles), and RV Tau (blue circles).

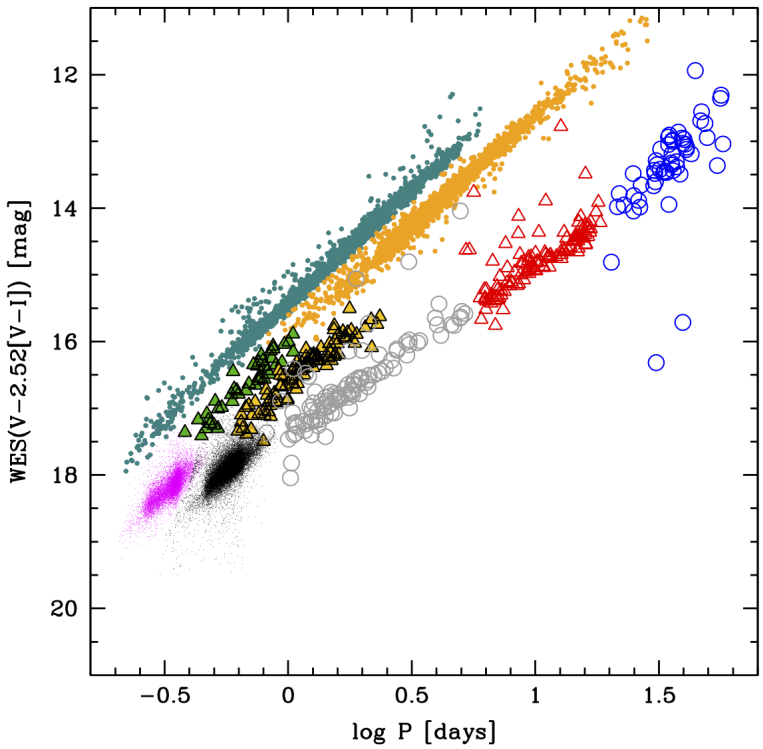

Figure 2. Wesenheit relations in V, I bands. Data and colour-code are the same than in Figure 1.

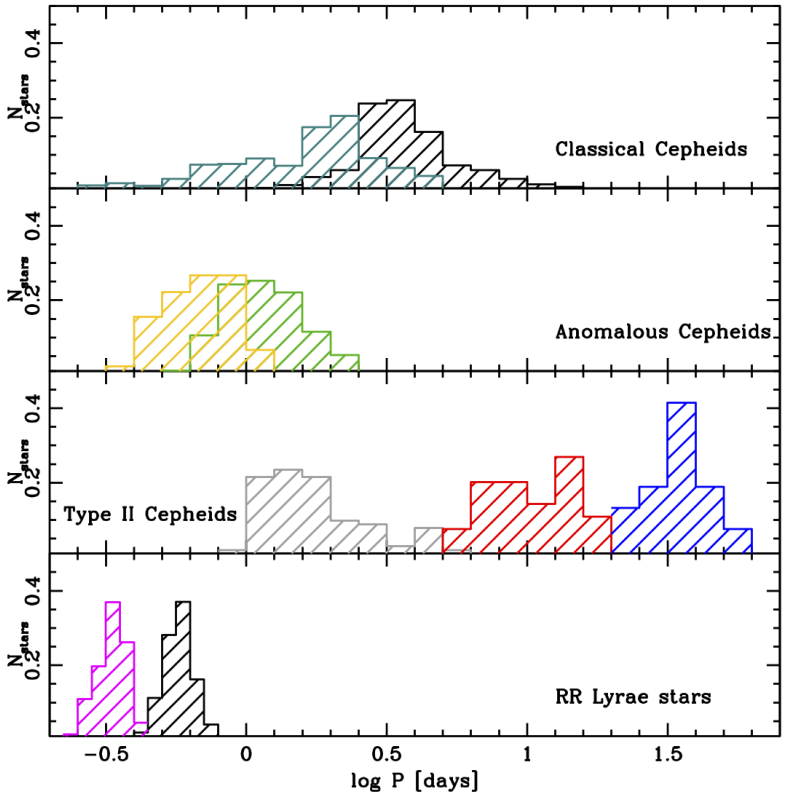

Figure 3. Period distribution of different types of pulsators. The data and the colour-code are the same as in Figure 1.

2.1. RR Lyrae Stars

RRLs stars populate the intersection of the IS with the Horizontal Branch (HB). They are therefore low-mass (0.6–0.8 $M_{\odot}$), relatively bright ($M_V \sim +0.5$ mag) stars burning He in their core. The RRL IS is well defined in colour, therefore in temperature, and limited to B–V colour between ∼0.2 and ∼0.8 mag (Walker [85]). The majority of RRL stars are known to pulsate either in the fundamental (FU or RRab) or in the first-overtone (FO or RRc) pulsation mode. The former are characterized by longer period (∼0.45 to ∼1 d), larger maximum amplitude (up to above 1 mag in the blue optical pass-bands), and asymmetric, saw-tooth-like light curves. RRc present on the other hand shorter periods (∼0.25 d to ∼0.45 d), amplitude barely reaching 0.7 mag in the visual, smoother and more sinusoidal light curves. Moreover, a fraction of RRL stars that ranges from few percents to 10%, depending on the mean metallicity of the host system, have been found to pulsate in both the fundamental and the first-overtone modes simultaneously (double pulsators or RRd). They typically have periods close to 0.4 d, small amplitude, and noisy light curves resulting from the superposition of the two modes (Braga et al. [86]).

RRLs have been observed in virtually all the stellar systems they have been searched for: in globular clusters, in the MW (halo, bulge, thick disk) and in the M31 (halo, disk) field, as well as in dwarf galaxies, with few rare exceptions such as very small mass spheroidal galaxies in the so-called ultra-faint regime (Vivas et al. [63]). For this reason, and given that they are primary distance indicators (see Section 4.5), they provide a complementary, population II route to calibrate the distance scale to estimate the Hubble constant, such as that investigated by the Carnegie-Chicago Hubble Program (Beaton et al. [87]).

The first discoveries of RRL stars outside the Milky Way (MW) dates back to Baade and Hubble [88], who reported the discovery of 40 variable stars in the Sculptor dwarf spheroidal (dSph) galaxy. However, it was only in the 50s when a significant number (200) of discoveries occurred (Thackeray [89]). Interestingly, RRL stars in the closer Magellanic Clouds were found

later, and by searching in their globular cluster system (Thackeray [90], Thackeray and Wesselink [91], Thackeray [92], Alexander [93]). While these first works (Baade and Swope [94], Nemec et al. [74], van Agt [95], Swope [96], van Agt [97], Hodge and Wright [98]) benefited from the wide-field provided by photographic data, they suffered from strong limitations on the limit magnitude. More modern instrumentation (digital sensor such as charged-coupled devices) allowed to overcome this problem, but with the price of a small area coverage. Variable stars have been searched for and investigated in all bright MW satellites (Martínez-Vázquez et al. [8], Coppola et al. [55], Siegel and Majewski [65], Nemec et al. [74], Kinemuchi et al. [76], Baldacci et al. [79], Bersier and Wood [99], Dall'Ora et al. [100]). In particular, the Magellanic Clouds have been targeted by microlensing project such as MACHO (Alcock et al. [101]), the subsequent implementations of the OGLE project (Udalski et al. [16], Soszyński et al. [102]) and, moving to the NIR regime, by the VMC project (Cioni et al. [21]). Also, since the beginning of the 2000s and thanks to large survey programs such as the SDSS (Sloan Digital Sky Survey) and DES (Dark Energy Survey), the number of faint MW satellites have dramatically increased, extending the range of properties to very low luminosity ($-6 < M_V < 0$ mag) and low metallicity ([Fe/H]~ -2). Interestingly, a significant fraction of these systems host a few RRL stars, despite the low mass (Vivas et al. [53]).

On the other hand, more distant galaxies such as those in the M31 system or isolated at the LG fringes require the use of 8–10 m class telescopes or the Hubble Space Telescope (HST) to reach the RRL stars with enough accuracy to study their luminosity variations. Indeed, the HST allowed to discover hundreds of variable stars, mostly RRL stars, in a sample of galaxies homogeneously observed (Bernard et al. [33], Martínez-Vázquez et al. [37], Monelli et al. [46], Bernard et al. [58,82]), while few other M31 satellites have been characterized with the Large Binocular Telescope (Cusano et al. [32,35,38,84]).

Finally, it has to be stressed that RRL stars have been found and characterized in only a few systems nearby, but outside, the LG: two galaxies in the Sculptor Group at $\sim$2 Mpc (Yang et al. [31], Da Costa et al. [103]), and three isolated systems: Leo P, (1.6 Mpc, McQuinn et al. [64]), VV 124 and KKr25 (1.3 and 2 Mpc, Neeley et al. [56]).

2.2. Classical Cepheids

Classical Cepheids (CCs) have period ranging from few to hundreds days and almost sinusoidal light curves[3].

As RRLs, most of them pulsate in the fundamental and the first overtone modes, but higher pulsation order are also observed (Soszyński et al. [29]) and are predicted by theory (Bono et al. [105]). CCs are brighter than RRLs (see Figure 1) and they are generally associated to intermediate mass stars. CCs are among the most popular primary distance indicators since the discovery of a well defined PL relation presented by Leavitt and Pickering [106] and based on the study of photographic plates of the Small Magellanic Cloud (SMC). They are in fact commonly used to calibrate SNIa with direct implication on the Hubble constant estimate H_0 and on the acceleration of the Universe (Riess et al. [107,108]). In particular, the metallicity dependency of their multi-band PL and Wesenheit relations is still matter of discussion and may have a significant impact on the final H_0 value (Fiorentino et al. [109], Marconi et al. [110], Macri et al. [111], Fiorentino et al. [112], Ripepi et al. [113], Breuval et al. [114]).

Based on their pulsation and evolutionary properties, CCs are also used as young stellar population tracers (100–300 Myr) since they obey to a well defined period-age relation (De Somma et al. [7], Marconi et al. [115]). This means that they can be safely used as tracers of the young components of a galaxy (disks/bars). The most famous and well studied CCs of the LG belong to the Large Magellanic cloud since they have been for long used to fix the zero-point of the Period-Luminosity (PL) relation (Macri [116], and references therein).

Among the dwarf galaxies of the LG, CCs in their full range of periods are present in a few massive and metal rich ([Fe/H] ≥ -1) dwarf galaxies: Magellanic clouds (Soszyński et al. [29], Soszyñski et al. [117]), M33 (Gieren et al. [118]). Lower mass classical dwarf galaxies ($M_V \leq -15$) with [Fe/H] ≤ -1 that show recent episodes of star formation

host mainly the short period tail of CCs (periods $\leq$ 10 d) with few exceptions, these are: LeoA (Bernard et al. [58]), IC1613 (Bernard et al. [33], Scowcroft et al. [119]), WLM, Sextans A and B, Pegasus (Tammann et al. [48], and references therein). As highlighted by Tammann et al. [48] and Bernard et al. [33], the Period Luminosity relations of short period CCs in dwarf galaxies differ from those observed in the LMC whereas they are similar to the SMC one, thus supporting a metallicity dependence of the PL relation. Furthermore, in their paper (Tammann et al. [48]) show a break in the PL relation at period ∼3.5 d. Thus, some care has to be devoted when using a universal PL relation for the short period CC sample.

2.3. Anomalous Cepheids

The definition of "anomalous" Cepheids was introduced by Zinn and Dahn [120] and Zinn and Searle [121] to remark the well-known observational evidence that Cepheids identified in MW dSph satellites obey a different PL relation than "normal" CCs and "cluster" (Population II) Cepheids (that is BL Her, W Vir, RV Tau stars). In particular, they were found in all dwarf galaxies (Thackeray [89], Baade and Swope [94], van Agt [95], Landi Dessy [122]) but only one in one GCs (Zinn and Searle [121]) and, at fixed period, they are less luminous than CCs (See Figure 2). These stars are characterized by periods ranging from ∼0.4 to ∼2.8 d, and light curves with shape and amplitude similar to RRL stars. Indeed, while it is relatively easy to distinguish them from RRL stars in external galaxies, their classification is not always easy in the field, especially if their light curve is not well characterized or the absolute magnitude is not well constrained (Plachy and Szabó [123]). Moreover, ACs overlap in the CMDs with the short-period tail of the CC period distribution. Therefore, since the pulsation properties of the corresponding pulsators (ACs or CCs) in the metal poor regime are very similar (Caputo et al. [124]), in order to properly identify the nature of Cepheids in a dwarf galaxy, a detailed comparison between evolutionary and pulsation models (as in Figures 4 and 5) and observations is always required.

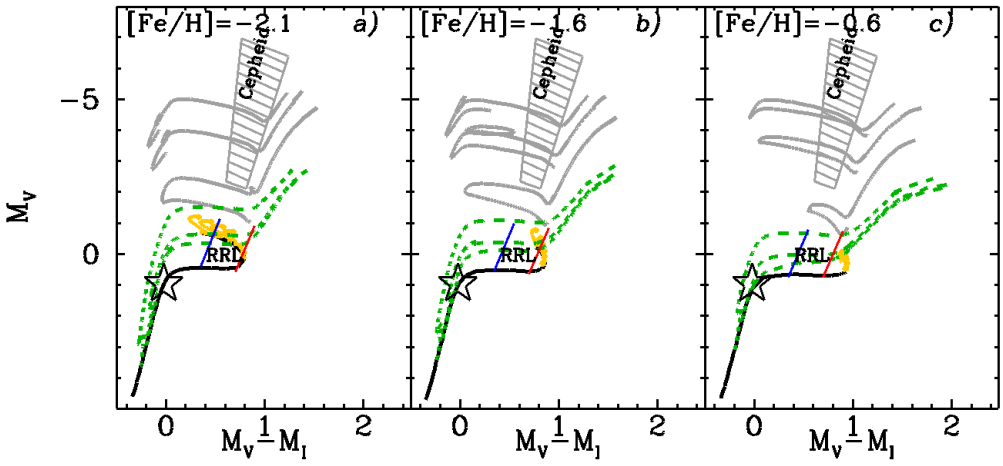

Figure 4. M_V, M_V-M_I Colour-Magnitude Diagram where the ZAHB loci for RRLs (black solid line), the evolutionary tracks for TIICs (green dashed lines), evolutionary tracks and HB loci for ACs (orange solid lines) and the CC blue loop phase (grey solid lines) are shown. The black empty star marks the empirical position of the extension to the blue of the HB for classical dwarf galaxies. The RRL (blue and red solid lines) and CC (grey dashed area) ISs are also shown.

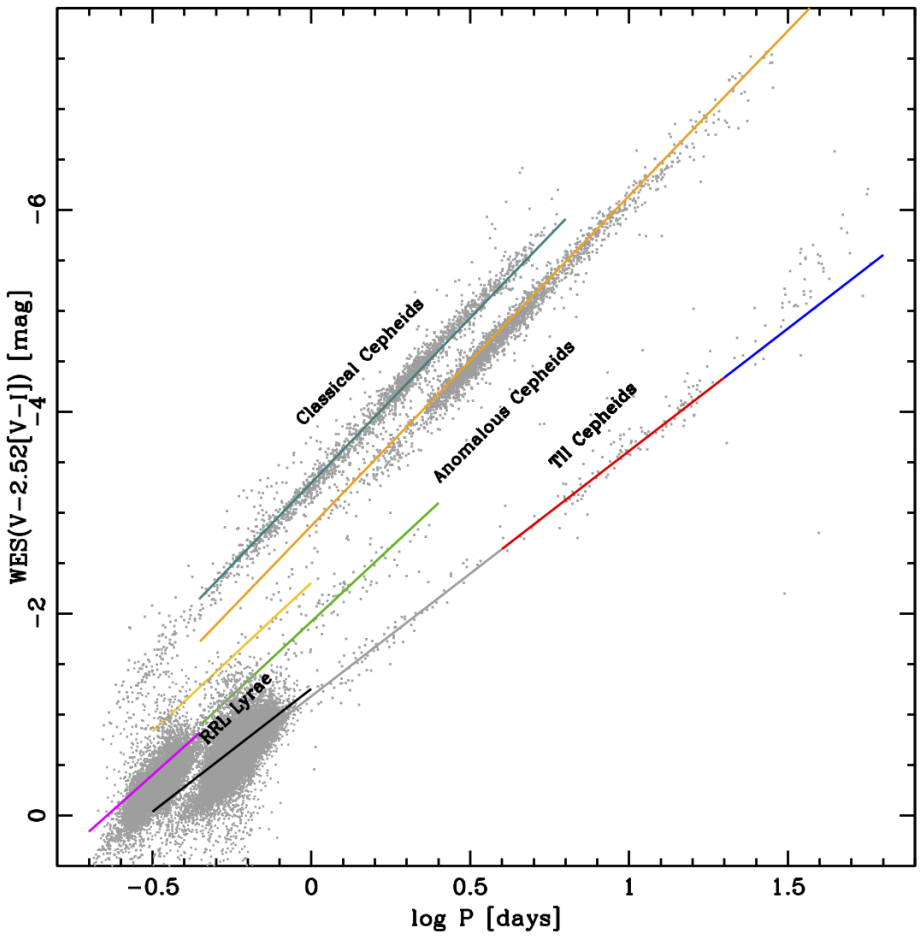

Figure 5. Theoretical Wesenheit relations in V, I bands colour-coded as in Figure 1. Data are also shown with grey dots.

ACs are present in small number in most bright LG dwarf galaxies. They have been observed in purely old systems (age $\geq$ 9–10 Gyr), such as in the dSph satellites Sculptor (3 ACs, Smith and Stryker [125]), Sextans (6, Mateo et al. [61]), LeoII (4, Siegel and Majewski [65]), Ursa Minor (7, Nemec et al. [74]), Draco (10, Harris et al. [126]), and also in isolated dSphs, like Cetus (8, Monelli et al. [34], Bernard et al. [82]), and Tucana (6, Bernard et al. [82]). However, they have also been found both in dSph galaxies with a large intermediate-age population (hereinafter, 1–6 Gyr), such as Fornax (17, Bersier and Wood [99]), Carina (20, Coppola et al. [55]) and in gas-rich dwarfs such as Phoenix (19, Gallart et al. [50], Ordoñez et al. [51]). The cases of Leo A and NGC 6822 are not as clear, for the coexistence of ACs and short period CCs (Baldacci et al. [79], Hoessel et al. [127], Dolphin [128]). A combination of both ACs and CCS is instead found in Leo I (Fiorentino et al. [129]), SMC, LMC (Soszyński et al. [43]).

Interestingly, such conditions can be fullfilled by stars evolving through two different evolutionary channels. In fact, they can either be relatively young $\lesssim$6 Gyr (Norris and Zinn [130]) or evolved binary systems where mass transfer has occurred (Renzini et al. [131], Wheeler [132], Gautschy and Saio [133]). Indeed, the second scenario can explain the existence of ACs in purely old dwarf galaxies, such as Sculptor, Ursa Minor, Draco or Sextans. On the other hand, both channels can be at work in galaxies with extended star formation history (Fiorentino and Monelli [134]).

2.4. Type II Cepheids

Type II Cepheids include three subgroups, namely BL Her, W Vir, an RV Tau. Observationally the distinction is empirically based on the period, which is shorter for BL Her (<4 d), intermediate for W Vir stars (4 to 20 d), and the longest for RV Tau. They are typical of GCs, the bulge, thick disk and the galactic halo, but are uncommon in dwarf galaxies. With the exception of the few hundreds stars known in the Magellanic Clouds (Soszyński et al. [45]) and 4 in the Sagittarius dSph (Hamanowicz et al. [78]), basically none are known in any other LG galaxy. Recently, Neeley et al. [56] reported the discovery of one BL Her in the isolated VV 124 galaxy.

They are thought to be old, low-mass, metal-poor stars (Wallerstein [135], but see also Iwanek et al. [136]), and are therefore interesting tracers of the halo (Wallerstein and Farrell [137]) and its building blocks (Prudil et al. [138]). Type II Cepheids also follow a PL relation (Feast et al. [139], Matsunaga et al. [140], Groenewegen and Jurkovic [141], Bhardwaj et al. [142]), and therefore can be used as distance indicators.

The three subgroups of Type II Cepheids are thought to sample different evolutionary phases (Gingold [143,144]). BL Her stars are thought to be low mass stars that evolve off the HB, moving towards the asymptotic giant branch (AGB) to higher luminosity and redder colour, and crossing the IS above the canonical position of RRL stars (Di Criscienzo et al. [145]). In their recent theoretical investigation Bono et al. [15] suggested the BL Her and V Vir share a common evolutionary channel, as the properties of the latter are compatible with being AGB stars crossing the IS during the blueward and redward path of the blue loop during the thermal pulses phase. The smaller mass and higher luminosity are the origin of the longer period with respect of RR Lyrae stars. Finally, RV Tau stars seem to be associated to post-AGB stars that are moving to the White Dwarf sequence, prior to the planetary nebula phase.

3. The Theoretical Scenario

Starting from the first simple models of radial stellar pulsation (Cox [146], Zhevakin [147]) it was clear that common mechanisms were driving radial stellar pulsation within the Classical IS. These mechanisms are associated to variation in the opacity (K-mechanism) and in the equation of state (γ-mechanism) within the stellar envelope, in the partial ionization regions of H, HeI and HeII (Cox [148]). Describing the stellar pulsation with leading physical arguments originally suggested by Ritter in 1879 (Ritter [149]), one can derive a simple relation between period (P) and mean density (ρ): P $\sqrt{\rho} \sim$ const. This fundamental equation can well predict stellar periods of all the radial pulsators described in this review. Radial envelope models can be used to predict the other pulsation observables such as blue and red edges of the IS, amplitudes. In particular, linear non adiabatic equations by following the pulsation growth-rate and the modal stability can predict the blue edge of the IS. Whereas pulsating amplitudes can be accounted for only by releasing the approximation of small oscillation and thus fully resolving the conservation equations (Bono et al. [150]). Finally, to predict the full set of observables, including the red edge of the IS, the convective transport has to be included in the physical description of the transport equation, since the increased efficiency of the convective transport quenches the driving mechanisms of radial pulsation (Stellingwerf [151], Bono and Stellingwerf [152], Gehmeyr and Winkler [153], Feuchtinger [154], Szabó et al. [155]).

To understand any period-luminosity/colour relations followed by the pulsating stars within the IS one can combine the simple Ritter equation with the Stefan-Boltzmann law for a black body emission to naturally derive the so called Van Albada & Baker relation (van Albada and Baker [156]), i.e., a relation between period and stellar luminosity, mass and effective temperature. Being stellar luminosity and mass strictly related to the chemical composition of the star, it seems obvious a dependence of the pulsating period from metallicity and helium abundance. Since in this section we will focus on the results obtained using an updated version of the Stellingwerf original code (Bono et al. [150], Stellingwerf [151]), here

we provide a recent formulation of the Van Albada relation provided in Marconi et al. [2] for RRLs:

$$logP_F = 11.347 \pm 0.006 + (0.860 \pm 0.003)logL/L_{\odot} - (0.58 \pm 0.02)logM/M_{\odot}$$
$$- (3.43 \pm 0.01)logT_e + (0.024 \pm 0.002)logZ \quad (1)$$

with slightly different coefficients, depending mainly on stellar gravity and on the assumed mass-luminosity relation, a similar relation holds for CCs (Bono et al. [157]), for TIICs (Di Criscienzo et al. [158]) and ACs (Marconi et al. [159]).

As clearly shown by the existence of the Van Albada & Baker relation, in order to model stellar pulsation we first need to properly identify the evolutionary state of variable stars, i.e., their mass and luminosity, and their initial chemical composition (Helium and metal mass fraction, Y and Z). Thus it is extremely important that the stellar evolutionary framework is also well understood. To help the reader in our discussion, we refer to Figure 4 where we show the location in the theoretical Colour-Magnitude diagram of the four main class of variables we are focusing on varying the chemical composition.

We note that the variable stars discussed in this review are in their central Helium burning phase or just after this phase. In Figure 4, the theoretical instability strip is shown by the blue and red solid lines (Marconi et al. [2]), while the Zero-Age Horizontal Branch (ZAHB) is plotted as a black solid line. RRLs are low mass ($M \leq 0.8\ M_{\odot}$) occupy the region where the ZAHB overlap with the IS. Type II Cepheids are lower mass stars in the off-ZAHB phase, evolving towards the *post-early AGB* phase (double shell burning) or *post-AGB* phase (hydrogen shell burning) as extensively discussed in Bono et al. [15]. Anomalous Cepheids are intermediate age mass stars ($\sim$1.3–2.3 $M_{\odot}$) in their central Helium burning phase (Fiorentino et al. [160]). All these three classes of variables ignite He in a degenerate core. Finally CCs have masses larger than previous groups ($\sim$2.2–12 $M_{\odot}$) and are centrally burning Helium in their core. Their larger masses allow the Helium burning ignition in a quiescent environment. During this phase intermediate mass stars move from the red to the blue part performing the so called Blue loop in the CMD (see grey evolutionary tracks in Figure), thus crossing the IS (grey dashed area).

Figure 4 shows three assumptions for the metallicity that brackets most of the LG dwarf galaxies' mean metallicity, ranging from [Fe/H] = -2.1 (left panel) up to -0.6 (SMC-like metallicity, right panel). This last assumption well represents also the evolutionary state of pulsating variable in the LMC. A glance at Figure 4 clearly shows that an increase in metallicity changes the path of evolutionary tracks across the IS. In particular, an increase in metallicity makes the RR Lyrae ZAHB move to fainter magnitude and redder colour, implying that the stars entering the IS have slightly lower masses and are fainter and thus they have shorter periods. Concerning TIICs, we have plotted three masses evolving from the blue part of the ZAHB, i.e., 0.52, 0.55 and 0.57 $M_{\odot}$ (dashed green lines). These cross the IS at lower luminosity when moving to higher metallicity. We have emphasized with an empty star (V–I~-0.02) the empirical blue limit attained by HB stars in LG dwarf galaxies. The missing blue tail of the HB makes TIICs very rare in dwarf galaxies, with very few exceptions SMC, LMC (Soszyński et al. [30]), VV124 (Neeley et al. [56]).

On the other hand, ACs are observed in basically all the LG dwarf galaxies brighter than $M_V \sim -8$. The evolutionary tracks that best account for their observed properties are plotted with light orange solid lines, and represent models with masses from $\sim$1 to $\sim$ 2 $M_{\odot}$. These tracks start from a sort of hook towards the blue of the ZAHB. For [Fe/H] = -2.1, the stars entering the IS have mass ranging from 1.2 to 2.0 $M_{\odot}$. For [Fe/H] = -1.6, the mass range shifts to between 1.8 and 2.0 $M_{\odot}$, whereas for [Fe/H] = -0.6, no star enter into the IS. This means that we can observe ACs only in very metal poor systems and as a such they trace very low metallicity stellar populations (Fiorentino et al. [160]). Finally, concerning CCs, we have plotted three masses, i.e., 3, 5 and 7 $M_{\odot}$ (grey solid lines). We see that at low metallicity the blue loop starts at higher effective temperatures (bluer colours), that is the where the central He burning is starting. Such a morphology implies that CCs

cross only one time the IS (first crossing) and thus they become more rarely observed at high luminosity and long periods. An increase in the metallicity implies a decrease in the effective temperature for the central He burning structure, but also a decrease in luminosity, this means more extended and fainter blue loops that cross twice the IS, i.e., more likely to be observed.

Once the evolutionary framework is settled, it can provide inputs for nonlinear pulsation models. In the last thirty years an extended grid of theoretical models have been provided, by using the updated version of the Stellingwerf code, for RRLs (Bono et al. [1], Marconi et al. [2], Bono and Stellingwerf [152], Bono et al. [161,162,163,164], Di Criscienzo et al. [165], Marconi and Minniti [166]), TIICs (Di Criscienzo et al. [145], Bono et al. [167], ACs (Marconi et al. [159], Fiorentino et al. [160], Bono et al. [168]), CCs (Fiorentino et al. [109,112], Bono et al. [157], Bono and Marconi [169], Bono et al. [170,171,172], Fiorentino et al. [173], Marconi et al. [174]). As an example of the good agreement between observation and predictions from theoretical models, we show in Figure 5 the Wesenheit relations obtained for the four classes of variables analysed and we compare them with data from LMC (see also description of Figure 2). We assume a distance modulus for LMC as given by Pietrzyński et al. [175] based on eclipsing binaries: $\mu_0 = 18.493$ mag. Theoretical models for RRLs (Marconi et al. [2]) and TIICs (Di Criscienzo et al. [145]) well reproduce slopes and zero points of LMC data. ACs also follow the theoretical relations (Marconi et al. [159]) once a mass of 1.25 $M_\odot$ is assumed. Finally, CCs show a similar slope but a different zero point, in fact we had to assume a distance modulus 0.16 mag longer in order to match theory and observation. This discrepancy has been explained with the uncertainty in the theoretical assumptions (Valle et al. [176]), i.e., the assumed Mass-Luminosity relation is affected by the uncertainty on the He core mass (rotation, mass loss, convection efficiency and other physical mechanisms are poorly known).

Since the theoretical models can reproduce not only the boundaries of the IS but the full amplitude variation along the pulsation cycle, one can model multiwavelength band light curve and then derive simultaneously distance and reddening. This method has been succesfully applied to RRLs and CCs (Marconi et al. [110], Marconi and Degl'Innocenti [177]). Another nice application of theoretical models is to derive the star formation history of the young component of a galaxy as traced by CCs (De Somma et al. [7,178,179]). Furthermore, the mass dependent Wesenheit relation for ACs can be used to constrain their pulsation stellar mass (Caputo et al. [124], see also Section 5. Finally one can combine evolutionary and pulsation predictions to interpret any observable of pulsating stars. As an example, in (Fabrizio et al. [180]), using their spectroscopic RRL Halo sample, they found a well defined behaviour of the relative number (N_{RRab}/N_{TOT}) as a function of the metallicity which has never been observed. This can be reproduced very well when using a combination of synthetic HB models and pulsation relations (Fiorentino et al. in preparation).

4. RR Lyrae Stars

RRL stars are considered the best tracers of old populations, and indeed their mere existence has been used as a proof for the existence of ancient populations in external galaxies (e.g., Leo A, Dolphin et al. [181]). Though the minimum age cannot be set theoretically, unless one makes the strong assumption that no mass loss occurs along the red giant branch (RGB), RRL stars are typically assumed to be older than 10 Gyr (Walker [85], Glatt et al. [182]). For this reason, they carry pristine information of the early condition of the host galaxy, and can be used to trace the first few Gyr of a galaxy's life.

4.1. RR Lyrae as Tracers of the Halo Formation

One important question regarding spiral galaxy formation concerns the build-up of their stellar halos which, according to cosmological simulations, are expected to grow from the accretion of smaller systems. However, the nature and size of these building blocks is uncertain and needs to be constrained observationally. The comparison of chemical patterns of RGB stars in the halo and surviving satellites (e.g., Venn et al. [183], Feltzing

and Chiba [184]) has been used for this goal, with somewhat inconclusive results since satellite dwarfs (may) have experienced extended evolution in comparison to the actual building blocks that merged to form the halos at a very early epoch. A purely old stellar tracer such as RRL stars can be used as a probe of the formation of the MW and M31 halos, by performing a comparison of the pulsation characteristics of these variable stars in the LG spiral galaxies halos, compared to dwarf galaxies and GCs. This was first done by Stetson et al. [60], who compared the properties of halo RRL stars (∼14,000 stars) to those of satellite dwarf galaxies (∼1300 stars) and globular clusters (∼1000). In particular, the period distribution of such large sample of RRL stars in different systems revealed that the distribution of the inner and outer halo (separated at 14 Kpc from the Galactic center) are not compatible to be drawn from the same parent distribution. This strongly suggests that the progenitors or types of progenitors had different nature. Second, the period distribution of dwarf galaxies can be different from that of the MW halo. This is shown in Figure 6, which present the period-amplitude diagram for different samples of stars in the MW halo (panel (b)), compared to bright (d) and faint (f) MW satellites. The corresponding period distributions are shown in panel (h). Focusing on the RRab stars, it shows clearly that bright and faint MW satellites present different properties.

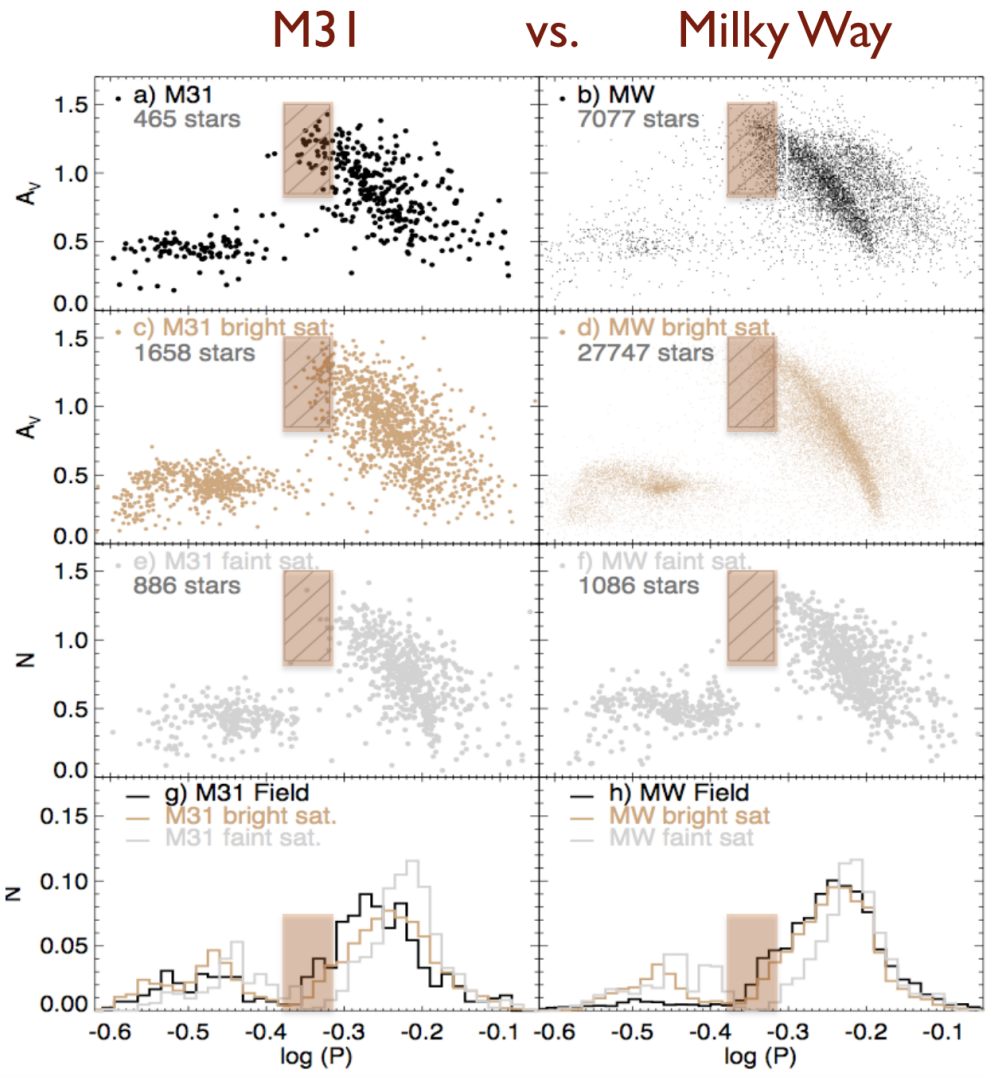

Figure 6. This Figure is adapted from Monelli et al. [36] and shows the period distribution and the Bailey diagram for RRLs in our Halo and in M31 as compared with the integrated distributions for faint and bright dwarf galaxies.

In particular, Fiorentino et al. [185] stressed that dwarf galaxies lack a specific population of RRL stars, that is the fundamental pulsators RRab with period smaller than P = 0.48 d and amplitude larger than A_V = 0.75 mag (shaded area in Figure 6). These High Amplitude Short Period (*HASP*) stars are on the other hand present in the MW halo and in globular clusters. In the same paper, the authors showed that the metallicity is playing a fundamental role. In fact, the period distribution of GCs clearly shifts toward shorter period for increasing metallicities of the clusters. As a consequence, only GCs more metal-rich than [Fe/H]~-1.4 host *HASP* RRL stars. This was confirmed using low-resolution spectroscopic metallicities of RRL stars from the SDSS (Drake et al. [20]). In fact, the Bailey diagram of the metal-rich sample clearly shows a shift toward shorter period when compared to the metal-poor ones.

On the other hand, *HASPs* are present in the most massive MW satellites, the Magellanic Clouds and the Sagittarius. This is reflected in the period distribution, and the evidence thus suggests two main conclusions:

1. the present-day MW dSph satellites are different from the objects that accreted to form the MW halo long ago;
2. the building blocks of the halo must have experienced an early and fast chemical evolution, that allowed them to produce a population of stars metal-rich enough to be detected today as *HASP* RRL stars. This suggests that the halo building blocks were massive systems.

Analogous results were found for the other large LG spiral, M31 (see left panel of Figure 6). Monelli et al. [36] using HST archival data, analyzed the population of RRL stars in three of the most massive M31 satellites (And VII, NGC185, NGC147), discovering more than 1500 new RRL stars. Among these, the three galaxies host a sizable fraction of *HASP* stars. On the other hand, smaller systems such those studied by the ISLAndS project (And I, And II, And III, And XV, And XVI, And XXVIII, Martínez-Vázquez et al. [37]), reveal a lack of metal-rich RRL stars similar to MW satellites of similar mass. Overall, the period distribution of the MW and M31 halo, despite the different size of the sample, show remarkable global properties. This supports the ideas that major mergers also played a relevant role in the early evolution of the M31 halo.

4.2. RR Lyrae and the Connection with the Host SFH

The classical morphological classification of dwarf galaxies divides most of the systems in spheroidal and irregular systems. The former are rounder, pressure-supported, gas-free, and preferentially old galaxies. The latter present more a clumpy structure, rotation, and a significant fraction of gas associated to current or recent star formation activity. In between, the somewhat ill-defined group of transition galaxies has intermediate properties. Indeed, the so-called morphology-density relation, that is the trend of dSph galaxies to be distributed closer to either the MW or M31 while the dwarf irregulars (with the exception of the Magellanic Clouds) tend to be more isolated at the fringes of the LG, suggest an evolutionary link with dIrr turning into dSph (Mayer [186]). In the end, this is the still open question about the "nature or nurture?" determining the dwarf galaxies evolution (Skillman and Bender [187]).

More recently, Gallart et al. [188] proposed a different scheme based on the full evolutionary history rather than the present-day, morphological properties. They collected star formation histories (SFH) obtained from deep CMD reaching well below the Main Sequence Turn-Off, which allow age resolution of $\sim$1 Gyr at the oldest epochs (12–13 Gyr, Gallart et al. [13]. The sample included MW satellites as well as isolated galaxies, and allowed to identify two groups of galaxies: (i) *fast* systems, which formed the vast majority or all the stars at old epochs (>10 Gyr, e.g., Cetus, Tucana, Sculptor, LGS3), and (ii) *slow* systems, with a fraction of old stars but a substantial or dominant intermediate-age to young populations. Interestingly, the slow/fast classification does not necessarily coincide with the dSph/dIrr one. In fact, systems like Fornax, Carina, and Leo I host a significant interemediate-age population but are dSphs. Moreover, the available orbits suggest that slow evolvers may

have entered the innermost region of the LG at relatively recent epochs. This suggests that slow galaxies may have formed in low-density environment, where the scarcity of accreting blocks would be responsible of the slow mass assembly, while fast systems would form closer to bigger galaxies, where the higher density would favour the quick assembly and the proximity to a larger galaxy would favor the quenching of the star formation.

RRL stars add extra information to this picture. As discussed in Fiorentino et al. [189], Figure 7 present the metallicity-luminosity relation for galaxies in the LG and its neighbourhood to ∼2 Mpc. Blue and red circles represent slow and fast galaxies, respectively, while filled and open symbols refer to the presence or absence of *HASP* RRL stars. The plot shows many interesting features. First, in the low-mass regime, no galaxies host *HASPs*, strongly suggesting a limited early chemical evolution. Note that while the vast majority of galaxies with $M_V > -11$ mag are fast, there are a few exceptions (Carina, DDO210, LeoT) with prolonged SFH host. Second, on the other extreme, among galaxies brighter than $M_V < -13.5$ mag, all host *HASPs*, again independently on the SFH. This supports the idea that they were initially massive enough to evolve quickly and reach [Fe/H]∼−1.4. Moreover, fast chemical enrichment in the most massive systems implies that the metallicity-luminosity relation was in place already at very early epoch.

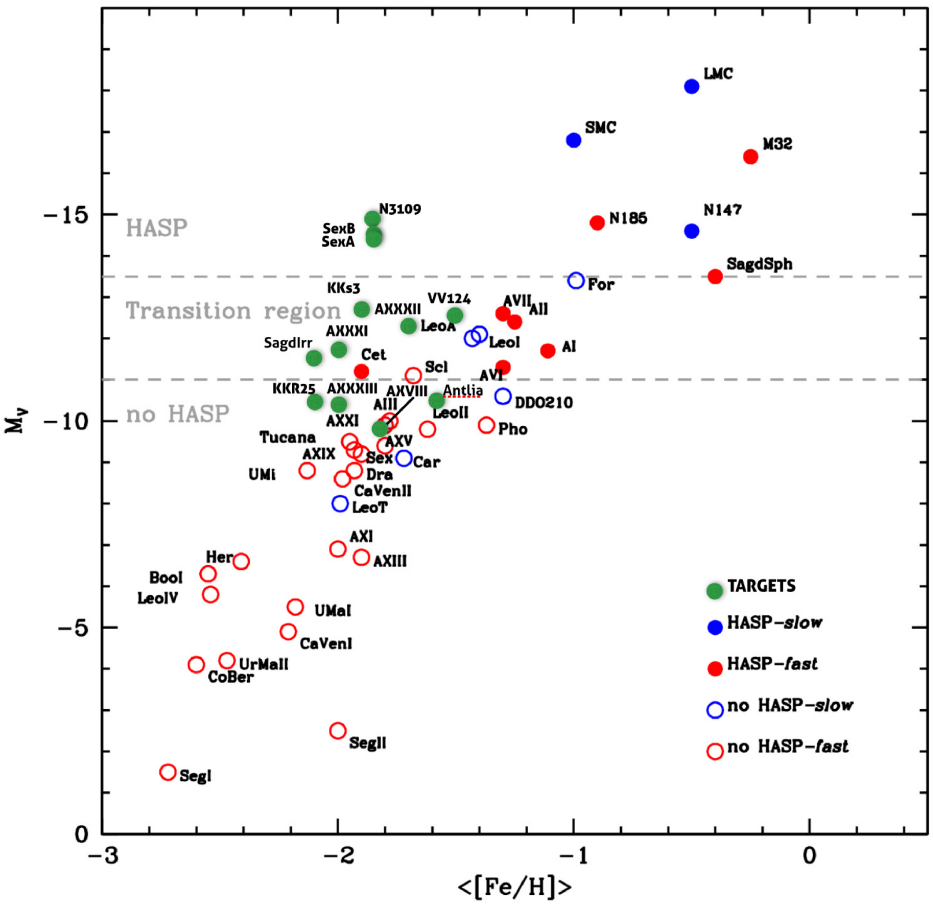

Figure 7. Luminosity-metallicity relation for galaxies within 2 Mpc for which RR Lyrae studies and SFH are available. The green symbols indicate interesting, relatively bright LG galaxies still lacking variability studies. This Figure has been adapted from Fiorentino et al. [189].

Third, there is a very interesting transition region in which fast galaxies do have *HASPs* (And I, AndII, And VII, Cetus, And VI) but slow dwarfs do not host any (Leo A, Leo I, Fornax). This suggests that the properties of RRL stars in this mass regime can provide fundamental information on the early SFH of the host galaxies. In this sense, the green symbols mark very interesting targets of nearby galaxies for which variability studies

and/or SFH are lacking. All are galaxies within 2 Mpc, for M31 satellites (And XXXI, And XXXIII) to isolated galaxies at the fringes of the LG (SagdIrr, And XVIII) or systems in the nearby NGC3109 group. The RRL stars in all these objects within the reach of HST, and could therefore be used as benchmark to test the early SFH in very different environments.

4.3. The Oosterhoff Dichotomy

Oosterhoff [190] was the first to recognize that GCs could be separated in two main groups, according to the properties of the period distribution of their RR stars. Quoting Oosterhoff: *"According to these figures the five clusters fall in two groups with a different distribution of their periods. The mean periods for the group of a- and b-type variables differ by as much as a tenth of a day"*.

The five clusters used for the discussion were M 3, M 5, M 15, M 53 and Omega Cen (see red squares in Figure 8). This evidence has been subsequently confirmed using the full sample of GCs hosting RRLs. In fact, the so-called Oosterhoff I clusters present shorter mean period (∼0.54 d and ∼0.32 d for the RRab and the RRc types, respectively) with respect of OoII cluster (∼0.64 d and ∼0.28 d). Also, the fraction of RRc is smaller in OoI clusters than in OoII ones. In addition, a third group has been proposed which includes the metal-rich clusters NGC 6388 and NGC 6441, characterized by higher metallicity and longer mean period. The Oosterhoff dicothomy therefore manifests with a different distribution of the RRL stars in the period-amplitude Bailey diagram, with the RRab on average occupying two different sequences shifted in period.

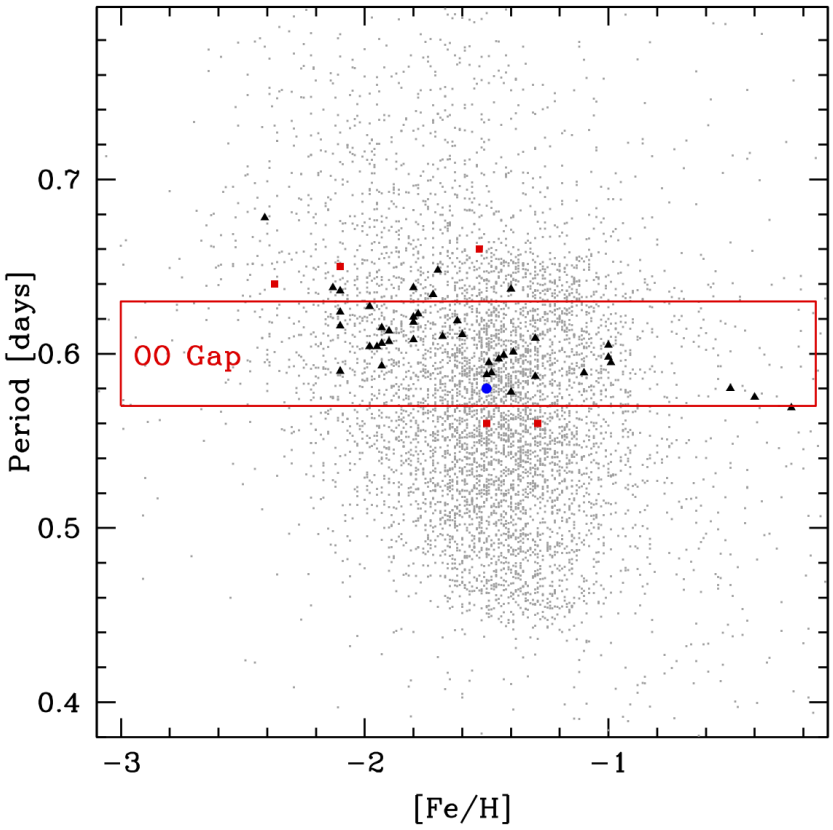

Figure 8. Period-metallicity diagram for field stars (grey dots, from Fabrizio et al. [180]), with superimposed the region of the Oosterhoff gap (red box). The blue dot shows the position of the mean value for all the MW stars. Black triangles and red squares show respectively the location of dwarf galaxies (from Table 1) and GCs (from the Clement catalogue, see http://www.astro.utoronto.ca/~cclement/cat/listngc.html accessed on 12 October 2021), plotting the mean period of the known RRL stars.

On the other hand, it is long known that nearby dwarf galaxies present different properties (black triangles in Figure 8). Indeed, the RRab stars in many systems tend to have mean period in the so-called "Oosteroff gap" (red box in Figure 8), that is close to 0.6 d and intermediate between the two man Oo-types. The Oosterhoff dichotomy puzzled scientists for more than 75 years and it has been long used to disclaim the role of dwarf galaxies in the formation of the Galatic halo. In fact, assuming that Halo properties can be well traced by GCs, the properties of RRab in dwarf galaxies do not follow the GC dichotomy. In the last years, a new spin to the Oosterhoff dichotomy has been provided by Fabrizio and collaborators (Fabrizio et al. [180,191]) as based on a large spectroscopic sample of Halo RRab. They have collected the largest and most homogeneous spectroscopic dataset of field RRLs available to date. They estimated abundances for 9015 RRLs using both high-resolution and low-resolution (ΔS method) spectra for fundamental (6150 RRab) and first overtone (2865 RRc). On the basis of this exceptional sample, they found that the pulsation period of both RRab and RRc variables steadily decreases when moving from the metal-poor to the metal-rich regime (see grey dots in Figure 8). An inspection of the plot clearly shows that the Halo RRLs cover the full region of the periods found in GCs and dwarf galaxies. The mean period of the Halo RRab is P $= 0.58 \pm 0.08$ d with a mean metallicity [Fe/H] = -1.50 ± 0.47 (blue dot) and appear at the short period edge of the OOsterhoff gap. However Halo RRab cover a very large range of periods spanning from short to long, thus the first conclusion we can draw is that averaged properties of RRab in GCs do not reproduce what is observed in field Halo stars. As a consequence, GCs can not be taken as representative of old field stars. Dwarf galaxies instead have mean period systematically longer than Halo stars, with few exceptions. These are LMC, Sagittarius and M32 that can be easily identified as the metal rich tail of the dwarf distribution. Andromeda VI is instead the classical dwarf with the shortest mean period (P $= 0.59$ d) and interestingly enough it is also the faintest galaxy hosting *HASPs* (see Figure 7). A glance at this figure clearly show that the mean period of RRab stars can not be used to probe the mean properties of Halo RRLs. One can draw as main conclusion that the Oosterhoff dichotomy in globular clusters is not reflected in the Halo. The GC dichotomy is due to the lack of a significant sample of metal-intermediate GCs hosting RRLs and is likely affected by the GC HB morphology.

4.4. RR Lyrae Stars as Early Chemical Evolution Tracers

Given that RRL stars formed during the first 2–3 Gyr of the life of the host galaxy, their metallicity distribution provides direct insight of the early chemical evolution of the system. The number of stars with high-resolution spectroscopic measurements has been increasing in recent years (see Crestani et al. [192,193], and references therein), but the trend is limited to nearby field stars only. So far, no direct spectroscopic measurements are available for RRL stars in external galaxies, with the exception of few low-resolution analysis in the LMC (Gratton et al. [194], Borissova et al. [195,196]) and Scultpor (Clementini et al. [197]). In all cases, the ΔS method (Preston [198]) was applied, inferring the metallicity from the equivalent width of the H Balmer lines and the Ca II K line.

To overcome this problem, alternative methods have to be searched, exploiting the fact that the pulsation properties of RRL stars are linked to their chemical composition. Therefore, different approaches have been suggested to derive the RRL metallicity from their light curves. Jurcsik and Kovacs [199] proposed a relation between the iron abundance, [Fe/H], and the ϕ_{31} parameter derived from the combination of two Fourier parameters. Alcock et al. [200] derived a period-amplitude-metallicity relation, while Sarajedini et al. [201] proposed a period-metallicity relation. These relations have been widely used to reconstruct the metallicity distribution of the RRL population of many LG dwarf galaxies (see e.g., Yang et al. [31], Pritzl et al. [83,202], Sarajedini et al. [203]). Indeed, they provide a cheap approach to overcome the complete lack of spectroscopic data of RRL stars in such systems.

More recently, Martínez-Vázquez et al. [8] and Braga et al. [204] proposed an alternative use of the PL relation in the I band (PLI) to derive individual metallicities of RRL stars in a stellar system. We will now discuss the application of this method to show the power of recovering RRL stars metallicities. The PLI relation connects the absolute magnitude, period, and metallicity of RRL stars (see below) and it is usually invoked to derive the distance. However, if an independent estimate of the distance of the host galaxy is available, for example from the RGB Tip or from a PL relation not involving the I-band, then it is possible to invert the equation (Marconi et al. [2]). This will provide individual metallicities and therefore the possibility to reconstruct the underlying distribution, which is in excellent agreement with the spectroscopic one (see the case of Sculptor, Martínez-Vázquez et al. [8]). Interestingly, when applied to a globular cluster with no intrinsic metallicity spread, the resulting distribution has a dispersion of the order of $\sigma_{[Fe/H]}$ ∼0.2 dex, which we can consider as the resolution of the method.

Figure 9 shows two examples of very different normalized metallicity distributions derived with the inverse of the PLI, for the Sculptor (Martínez-Vázquez et al. [205]) and Crater II (Vivas et al. [70]) dwarf galaxies. Sculptor presents a significant metallicity spread, estimated as the sigma of the distribution, of the order of σ ∼0.35 dex, which strongly suggests that Sculptor was able to retain the yields of Supenovae associated to the first events of star formation, causing the mean metallicity to increase on a time scale shorter than 2 Gyr. This is strongly supported by the luminosity spread of RRL stars, and the complex distribution of stars in the Bailey diagram. On the other hand, Crater II presents a metallicity distribution compatible with no intrinsic dispersion.

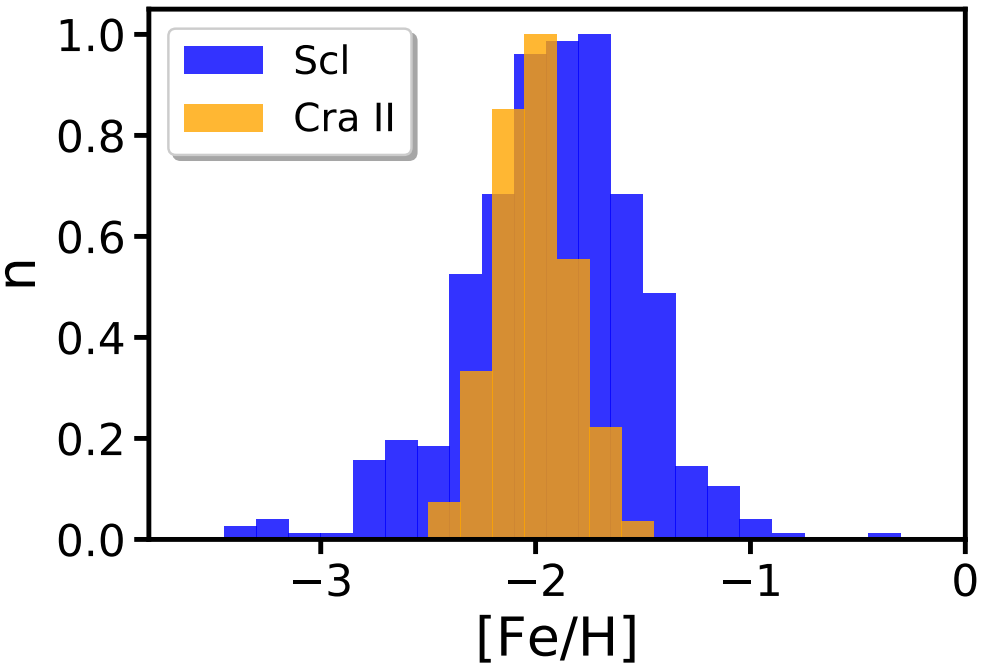

Figure 9. Metallicity distribution derived with the PLI relation for the RRL stars in the Sculptor and Crater II dwarf galaxies.

The comparison with the metallicity distribution of the RGB stars provides interesting clues. In the case of Sculptor, Martínez-Vázquez et al. [8] shows that the global metallicity distribution of RRL and RGB stars covering a substantial fraction of the galaxy is in excellent agreement. On the other hand, when restricting to the innermost regions only, the RGB stars provide a higher number of higher metallicity objects. This is reflecting the spatial gradients of the different stellar populations. As commonly seen in most LG dwarf systems (Harbeck et al. [206]), the star formation was more prolonged in the innermost regions than

in the external ones. This is also reflected in an average increase in metallicity toward the central regions. Sculptor followed this outside-in trend, with the star formation stopped earlier in the outskirts (10 Gyr ago) than in the center (6 Gyr, de Boer et al. [207]). Therefore, the RGB stars reflects a broader age and metallicity range than the purely old population traced by RRL stars. Interestingly, in the case of Crater II, RRL and RGB stars provide similar dispersion, suggesting both a limited spread in age and metallicity, suggesting that the star formation was quenched before 10 Gyr ago.

A limit of this technique is that it cannot be used to simultaneously derive both the distance and the metallicity. However, this can be done whenever BVI photometry is available. In fact, the Wesenheit (V, B–V) PL relation (which is not only, by construction, reddening-free, but also largely metallicity independent, see below) can be used to derive the distance, and then the PLI can be used to derive the metallicity distribution of RRL stars (see for example an application to Crater II in Monelli et al. [69]), and also an independent distance estimate for comparison. Figure 9 illustrates that dwarf galaxies show diverse early evolution, but the landscape is much more complex, as reflected by the period-amplitude (Bailey) diagram. Figure 10 shows selected Bailey diagrams for 9 dwarf galaxies, including MW (Carina, Sculptor, and Fornax, top line) and M31 (And III, And II, and And XXVIII, middle line) satellites, and isolated systems (Cetus, Tucana, VV 124, bottom line). The plot at first sight shows that it is impossible to associate dwarf galaxies to the Oosterhoff types usually used for GCs (see Section 4.3), represented by the red lines (dashed and solid lines for the Oosteroff I and II type, respectively, from Fabrizio et al. [191]). First, the sequence of RRab type stars is narrower in some case, and somehow closer, but steeper, than the Oo-I locus (dashed line). This occurs for the three galaxies in the left column, that is Carina, And III and Cetus. We argue that this reflects internally homogeneous properties (Monelli et al. [34]), with no metallicity spread associated. Indeed, galaxies with complex RRL populations, such as Tucana (Bernard et al. [208]), And II (Martínez-Vázquez et al. [37]) and Sculptor (Martínez-Vázquez et al. [205]), present a broader RRab sequence, with a large period spread at fixed amplitude, which can be ascribed to an instrinsic metallicity dispersion. Finally, the right column shows the larger galaxies Fornax (Fiorentino et al. [189]) and VV 124 (Neeley et al. [56]), together with the peculiar And XXVIII (Martínez-Vázquez et al. [37]). It should be noted that the present-day properties of the RRL stars do not correlate with the environment where the host galaxy is currently located. In fact, galaxies hosting simple or complex RRL samples are present in the surroundings of the MW and M31 but also in isolation.

Finally, we stress that photometric approaches to derive the metallicity distribution of RLL stars such as the PLI or the Fourier decomposition (see Mullen et al. [209] for a recent calibration) are especially powerful for distant galaxies (1–2 Mpc) currently within the reach of the HST, and for more distant galaxies which can be targeted by future facilities such as the James Webb Space Telescope. For these systems, the spectroscopy of the RGB stars is at the limit or outside the reach of current instrumentation, and the turn-off of the oldest population cannot be measured, thus limiting the age resolution of the SFH (Gallart et al. [13]). Therefore RRL stars offer a unique path to access the early evolution of these systems.

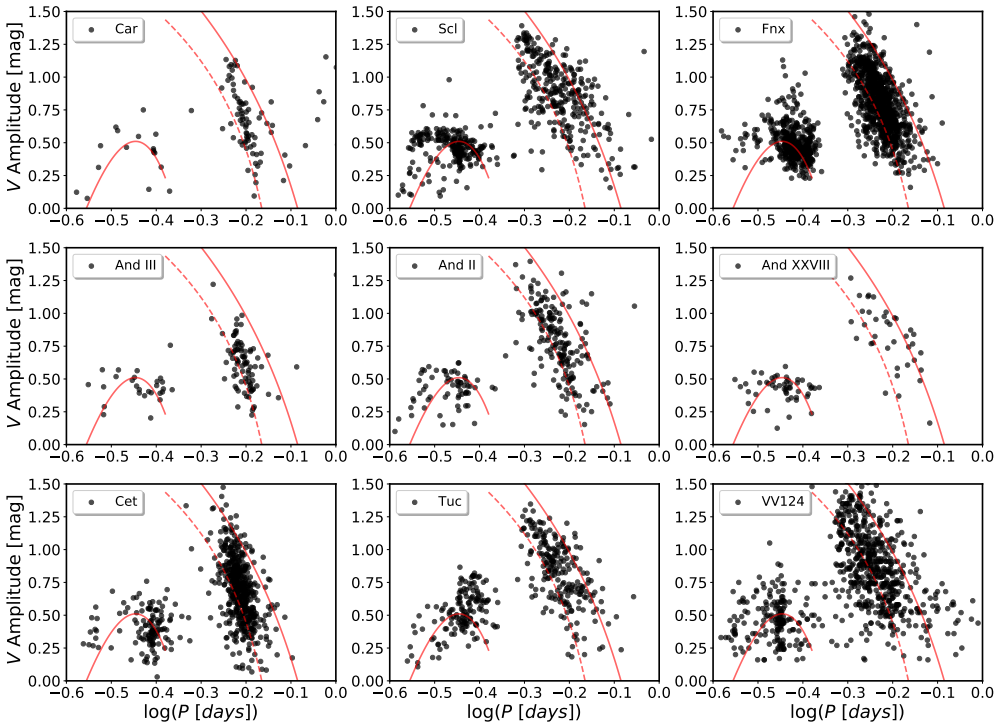

Figure 10. Bailey diagram for selected LG galaxies. See text for details.

4.5. RR Lyrae Stars as Distance Indicators

RRL stars are primary distance indicators and have a fundamental role in the establishment of the cosmic distance ladder for a number of reasons: (i) they are population II tracers, and therefore provide an independent route to H_0 with respect to younger stars such as Classical Cepheids; (ii) They are more numerous and present in a larger number of environments than CCs; (iii) with the current observational facilities they are detectable till outside the edge of the LG, to ∼2 Mpc Yang et al. [31], Neeley et al. [56], McQuinn et al. [64], Da Costa et al. [103]). Moreover different, independent methods can be applied to exploit the pulsational properties of RRL stars to derive the distance of the host system. We discuss here the Metallicity-Luminosity relation, and the Period-Luminosity-Metallicity (PLZ) relations.

4.5.1. Metallicity-Luminosity Relation

It has long been known that the luminosity level of the RRL stars depends on the metal content, given that it is set by the mass of the He core which in turn primarily depends on the metallicity (the higher the metallicity, the smaller the core mass, the fainter the star on the HB, see also Figure 4). Indeed, a linear relation of the form

$$\mathrm{M}_V = a + b \cdot [Fe/H] \tag{2}$$

was proposed, where M_V is the mean absolute magnitude in the V-band and [Fe/H] the mean metallicity of the RRL sample (Sandage [210,211]). The simplicity of this relation has made of it the most used method to derive the distance of GCs (e.g., Walker [212], Walker and Mack [213]) and LG galaxies. Indeed, basically all galaxies with detected RRL stars have distance estimate based on this method (e.g., Bernard et al. [33], Cusano et al. [38], Sarajedini et al. [201]).

Nevertheless, the available estimates are far from being homogeneous, as this relation presents a large number of conundrums that have to be taken into account:

- *Evolutionary Effects:* stars in the HB spend only a minor fraction of the evolutionary time close to the ZAHB, as they evolve to higher luminosity while the central He burning proceeds. Therefore, as is not possible to know in detail the evolutionary

status of each star, the observed mean magnitude, which is typically assumed, may not be the best to represent the ZAHB luminosity of the RRL stars population. This is also the main reason why this relation cannot be inverted and applied to individual stars to derive their distance.

- *Metal content 1:* Direct high-resolution measurements of the metallicity in external galaxies is still lacking at present time. Therefore, when using the Metallicity-Luminosity relation, an assumption of the metal content has to be done. This can be safely done for the vast majority of (typical) globular clusters, characterized by null or negligible spread in metallicity, which can be safely measured in RGB stars. This is not true in the case of dwarf galaxies, which show a complex mix of stellar populations with different ages and metallicities. As a further complication, metallicities in dwarf galaxies are typically derived for bright RGB stars. However, galaxies often host populations of stars too young and/or too metal-rich which do appear in the RGB, but they do not have a counterpart in the RRL population. For this reason, blindly assuming the global spectroscopic metallicity from the RGB can bring to an overestimation of the RRL metallicity introducing a systematic in the distance determination. To overcome this, assumption have to be made on the metallicity of the RRL stars, or alternative, direct estimate of the metallicity from the RRL pulsational properties can be performed (see Section 4).
- *Metal content 2:* Another issue related to the metal content is that the population of RRL can present an *intrinsic* spread in metallicity, due to a fast self-enrichment occurred on a 1-2 Gyr time scale. This is for example the case of Tucana (Bernard et al. [208]), Sculptor (Martínez-Vázquez et al. [205]), or the LMC (Skowron et al. [214]).
- *Reddening:* line-of-sight extinction directly affects the apparent mean magnitude of RRL stars, and therefore systematically shifts the distance estimate, mimicking fainter and therefore more distant RRL stars. Moreover, differential reddening artificially inflates the magnitude spread, also affecting the mean magnitude determination;
- *Linearity:* both empirical and theoretical works have suggested that the relation is quadratic rather than linear or, possibly, it presents a break close to [Fe/H] = -1.5, being steeper at lower metallicities (Bono [215]). Nevertheless, there is no consensus yet on this point (Muraveva et al. [216]).
- *Calibration:* nevertheless, the most basic and possibly the important problem of the Metallicity-Luminosity relation is the calibration of its coefficients, which is still not well established.

Concerning the last point, the data provided by the Gaia satellite are expected to provide a definitive answer to the calibration of the distance relation. Muraveva et al. [216] first calculated the zero point and slope of the Metallicity-Luminosity relation, using field stars with available spectroscopic metallicity (Dambis et al. [217]) and parallaxes from the Gaia DR2. In Figure 11 we provide a comparison of the distance using different calibration of the same relation. We take as reference the linear calibration obtain by Muraveva et al. [216] with the sample of 381 stars, derived recalculating the value of the systematic Gaia parallax offset (-0.062 mas, first line of their Table 4). The top panel shows the difference between the distance modulus calculated with the assumed Muraveva calibration and the distance modulus calculated with other calibrations available in the literature (see caption for details). The distance values are homogeneously derived assuming the same mean $< V >$ magnitude and the same mean metallicity of the RRL stars, so the difference displayed in the figure depend only the assumed calibration, and not on other parameters affecting the absolute value of the distance, such as the reddening.

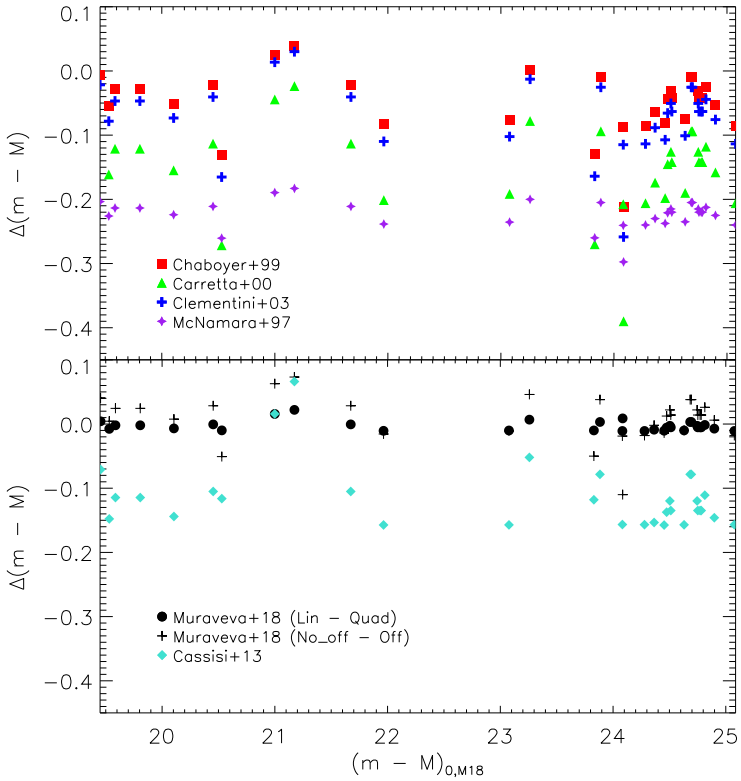

Figure 11. Comparison between the distance modulus determined with different calibrations of the MLR. Symbols refer to Chaboyer [218] (red squares), Carretta et al. [219] (green triangles), Clementini et al. [220] (blue pluses), and McNamara [221] (purple stars).

The plot discloses that the different calibration provide systematic difference ranging from −0.04 mag (median value) in the case of Chaboyer [218] to −0.21 mag for McNamara [221]. In particular Gaia DR2 derives smaller distance modules, hence shorter distances. The bottom panels present in black the comparison between different relations derived by Muraveva et al. [216]. Adopting the same reference relation, we compare the derived distances with the linear relation which assumes the parallax offset by Arenou et al. [222] (−0.057 mas, black pluses), and the quadratic one (black circles). The light blue symbols show the comparison with the quadratic relation by Cassisi and Salaris [223], which again gives systematically longer distances (−0.13 mag). Figure 12 shows the same comparisons, but shown as a function of metallicity. The plot clearly allows to visualize the effect of the different metallicity slopes assumed. Table 2 lists for 33 galaxies the adopted reddening, metallicity, and presents in column 4 the distance derived with the linear relation by Muraveva et al. [216].

Recently, Nagarajan et al. [224] presented the distance to 39 LG galaxies based on literature data, applying a PLZ relation anchored to 35 field RRL stars with spectroscopic metallicities and parallaxes from Gaia DR3. They found distances that are on average shorter with respect of the literature value. Figure 13 shows the comparison with the distance derived with the ML relation by Muraveva et al. [216]. For homogeneity, we applied the latter assuming the metallicity reported in Table 4 of Nagarajan et al. [224]. The plot shows that there is a small systematic difference of −0.06 mag (in the sense that the ML relation provide longer distances), but there is a large spread of 0.24 mag.

Though still preliminary, this exercise shows that (i) distance values in the literature are highly inhomogeneous, and should be treated cautiously; (ii) we are approaching, but we are still far from a solid, self-consistent calibration of the distance across LG galaxies. A crucial ingredient to anchor the calibration is the availability of high-resolution spectro-

scopic metallicities for a larger number of nearby RRL, for which Gaia will provide the best parallaxes.

Table 2. Adopted reddeding, mean metallicity and mean $< V >$ magnitude to derive the distance to 33 LG galaxies. See Figure 11.

Galaxy	E(B–V)	[Fe/H]	$< V >$	References
Ursa Minor	0.032	−2.13	19.90 ± 0.07	Nemec et al. [74]
Draco	0.027	−1.93	20.10 ± 0.10	Kinemuchi et al. [76]
Sextans	0.047	−1.93	20.32 ± 0.12	Vivas et al. [53], Mateo et al. [61]
Sculptor	0.018	−1.68	20.13 ± 0.09	Martínez-Vázquez et al. [47]
Carina	0.061	−1.72	20.69 ± 0.12	Coppola et al. [55]
Crater 2	0.030	−1.98	20.95 ± 0.01	Vivas et al. [53], Joo et al. [68], Monelli et al. [69]
Hercules	0.062	−2.41	21.35 ± 0.03	Musella et al. [75]
Fornax	0.021	−0.99	21.36 ± 0.15	Braga et al. in prep.
Leo 4	0.026	−2.54	21.48 ± 0.03	Moretti et al. [67]
CanesVenatici1	0.014	−1.98	22.17 ± 0.02	Kuehn et al. [73]
Leo 1	0.036	−1.43	22.65 ± 0.01	Stetson et al. [60]
Leo T	0.005	−2.20	23.68 ± 0.08	Surot et al. in prep.
Phoenix	0.016	−1.49	23.74 ± 0.12	Ordoñez et al. [51]
NGC 6822	0.231	−1.00	24.66 ± 0.17	Baldacci et al. [79]
Andromeda XVI	0.067	−2.10	24.34 ± 0.07	Martínez-Vázquez et al. [37]
Andromeda XV	0.047	−1.80	25.07 ± 0.07	Martínez-Vázquez et al. [37]
Andromeda II	0.061	−1.39	24.78 ± 0.09	Martínez-Vázquez et al. [37]
Andromeda XXVIII	0.090	−2.10	25.14 ± 0.08	Martínez-Vázquez et al. [37]
Andromeda XI	0.080	−1.80	25.31 ± 0.02	Yang and Sarajedini [42]
Andromeda I	0.053	−1.45	25.13 ± 0.10	Martínez-Vázquez et al. [37]
Andromeda III	0.056	−1.78	25.04 ± 0.09	Martínez-Vázquez et al. [37]
IC 1613	0.025	−1.60	24.99 ± 0.01	Bernard et al. [33]
Cetus	0.028	−1.90	25.03 ± 0.01	Monelli et al. [34]
Andromeda VII	0.194	−1.40	25.77 ± 0.13	Monelli et al. [36]
Andromeda VI	0.063	−1.50	25.29 ± 0.03	Pritzl et al. [83]
Leo A	0.021	−1.40	24.97 ± 0.04	Bernard et al. [58]
M32	0.154	−0.25	25.17 ± 0.18	Fiorentino et al. [40]
Andromeda XXV	0.101	−1.90	25.27 ± 0.09	Cusano et al. [35]
Andromeda XIX	0.062	−1.80	25.34 ± 0.10	Cusano et al. [32]
Andromeda XXVII	0.040	−1.70	25.24 ± 0.06	Cusano et al. [38]
Andromeda XXI	0.093	−1.80	25.33 ± 0.11	Cusano et al. [84]
Andromeda XIII	0.082	−1.70	25.49 ± 0.02	Yang and Sarajedini [42]
Tucana	0.031	−1.95	25.32 ± 0.01	Bernard et al. [82]

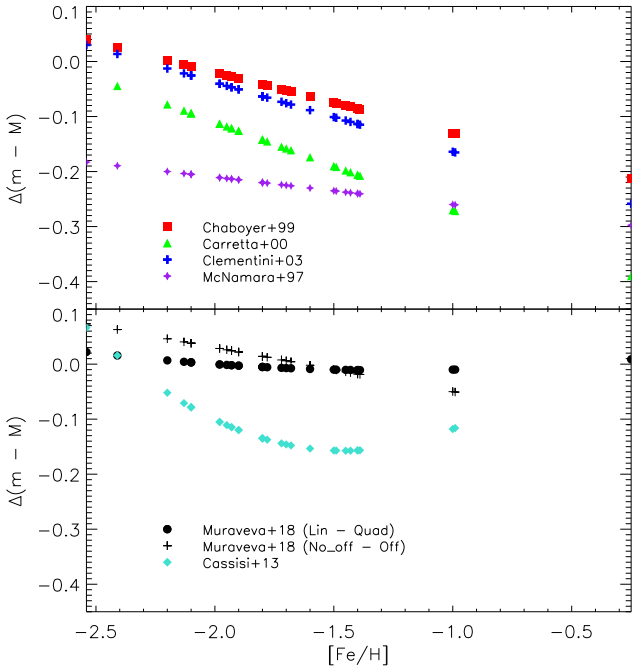

Figure 12. Same as Figure 11, but the comparison is shown as a function of metallicity.

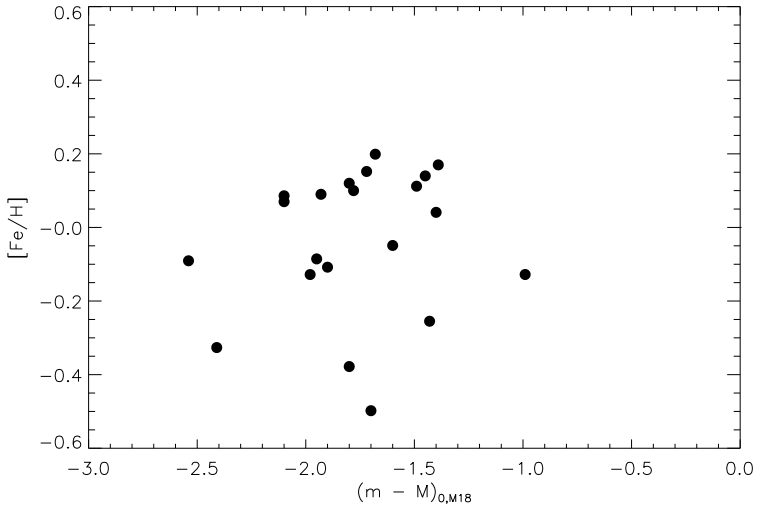

Figure 13. Same as Figure 12, but the comparison is shown with Nagarajan et al. [224] for the galaxies in common.

4.5.2. Period-Luminosity-Metallicity Relation

The M_V-[FeH] relation has been largely applied to LG galaxies. Indeed, basically all LG galaxies have a distance estimate with this technique. On the other hand, it is only thanks to the pioneering observational work by Longmore et al. [225], decades after the discovery of the PL for Cepheids, that RRL stars were found to a PL relation at infrared wavelengths. The PL originates from the increase of the period when moving from the blue to the red edge of the IS, as a consequence of the change in temperature. However, while M_V remain nearly constant within the IS because the bolometric correction has negligible dependence on the temperature, this is not the case in the *K* band, where the bolometric correction makes cooler stars brighter in the same temperature range. The combined effect produces a PL with slope close to −2.2 (Bono et al. [226,227]).

Moreover, the near and mid-infrared wavelengths have notable advantages when compared to the optical regime (Madore et al. [228]): the effect of reddening is significantly decreased, as well as the evolutionary effects, and the light curves are more symmetrical and therefore less phase points are needed to characterize them (Braga et al. [229]). Therefore, this approach is particularly appealing because future facilities such as James Webb Space Telescope and the Extremely Large Telescopes, which will be equipped with NIR cameras, will allow to extend variability studies well beyond the LG. As a drawback, the smaller amplitude could hamper the detection, especially in crowded region and for the RRc type stars.

The work by Longmore et al. [225] prompted numerous empirical investigations in GC (e.g., Dall'Ora et al. [230], Sollima et al. [231], Muraveva et al. [232]), but only a handful of galaxies have distance derived using *JHK* photometry of RRL stars, started by the Araucaria collaboration: Sculptor (Pietrzyński et al. [233]), LMC (Szewczyk et al. [234]), SMC (Szewczyk et al. [235]), Carina (Karczmarek et al. [236]), and Fornax (Karczmarek et al. [237]), for which the distance estimate was based on the PL in the *K* band. Hatt et al. [238] used optical (ACS) and NIR (WFC3) HST data to derive the distance to IC 1613 using PL and Wesenheit relations based on different bands combinations. Also, we have to stress the huge observational effort by program such as the VVV-VISTA Variables in The Via Lactea (Minniti et al. [22]), and VMC-VISTA survey of the Magellanic Clouds system (Cioni et al. [21]), which produced time series NIR data for the galactic disk and bulge (Dékány et al. [239], Contreras Ramos et al. [240]), and the Magellanic Clouds (Muraveva et al. [241], Cusano et al. [242]).

Recently, the PLZ relation is getting increasing popularity (e.g., Martínez-Vázquez et al. [205], Nagarajan et al. [224]), both thanks to the recent theoretical

works by Marconi et al. [2,243], and the vigorous interest and expectations connected to Gaia (Bhardwaj [244], Marconi et al. [245]) and the geometric calibration of the distance relations.

5. Anomalous Cepheids

5.1. On the Origin of ACs

The observational properties of ACs, that have similar period but higher luminosity with respect of RRL stars, immediately suggested mass larger than the typical one of RRL stars (Christy [246], Demarque and Hirshfeld [247]). ACs were suggested to be stars close to $\sim$1.5 $M_{\odot}$, metal-poor enough to enter the IS during the central He-burning phase. Indeed, the occurrence of such a class of variables is strictly connected to position of the He core transition mass in the CMD. M_{HeF} is defined as the transition mass between stars that ignite helium in the center under partial degenerate condition (smaller masses) or in a quiescent way (larger masses, see Fiorentino et al. [129] for an exhaustive discussion). M_{HeF} does not depend on the galaxy metallicity (for [Fe/H] ≤ -0.7) and it is fixed at $\sim$2.1 $M_{\odot}$. However, its location in the CMD depends on the metallicity, and the crossing of the IS occurs only for [Fe/H] ≤ -1.3. As a consequence, ACs are very good tracers of a low metallicity stellar population in the host system.

Even though ACs identify a population of stars in a well-defined mass range (1.3–2.1 $M_{\odot}$), the nature of their progenitors is still being debated. If they are the result of the evolution of single stars, then they trace a relatively young event in the star formation, which occurred from $\sim$1 to 6 Gyr ago (Zinn and Searle [121], Demarque and Hirshfeld [247], Castellani and degl'Innocenti [248], Caputo et al. [249]). On the other hand, it has been proposed that they are the evolution of blue straggler stars, formed via mass-exchange in old binary systems (Renzini et al. [131], Wheeler [132], Gautschy and Saio [133], Sills et al. [250]) that survived in low-density environments. In this case ACs would be tracers of the old and metal-poor population.

In order to better understand the origin of ACs, Fiorentino and Monelli [134] made a statistical spatial analysis exploiting the large sample of ACs in the LMC. They showed that ACs do not follow the same spatial distribution of CCs. This and the difference in their PL relations further supported the hypothesis that ACs are not the extension to low luminosity of CCs. The spatial distribution of ACs was also found to be different from that of bona-fide tracers of the old population, such as RRLs and TIICs, suggesting that the majority of ACs in the LMC are intermediate-age (1–6 Gyr), metal-poor single stars. This is supported by Figure 14, which shows the frequency of ACs as a function of the luminosity of a sample of LG galaxies. The plot, originally proposed by Mateo et al. [61], updates the results from Fiorentino and Monelli [134] and connects to the evolutionary properties of the target galaxies, in terms of fast and slow evolvers defined in Section 4.2. Figure 14 includes now 26 galaxies (10 more than in Fiorentino and Monelli [134]) and it shows that fast evolvers follow a very tight relation (red symbols), with the AC frequency decreasing for increasing luminosity of the host system. Slow galaxies (blue symbols), characterized by strong intermediate-age and young star formation, follow a different relation with similar slope but shifted to higher frequency values. This means that, at fixed luminosity, slow galaxies tend to have more ACs, in agreement with the fact that they can produce them both via the single and binary star channels.

$$logS = 3.18 + 0.35(\pm 0.04)M_V\sigma = 0.20 \quad fast\ \ evolvers \tag{3}$$

$$logS = 3.69 + 0.33(\pm 0.08)M_V\sigma = 0.37 \quad slow\ \ evolvers \tag{4}$$

Equations (3) and (4) list the fitting linear relations for the two groups of galaxies, disclosing very similar slope between the two.

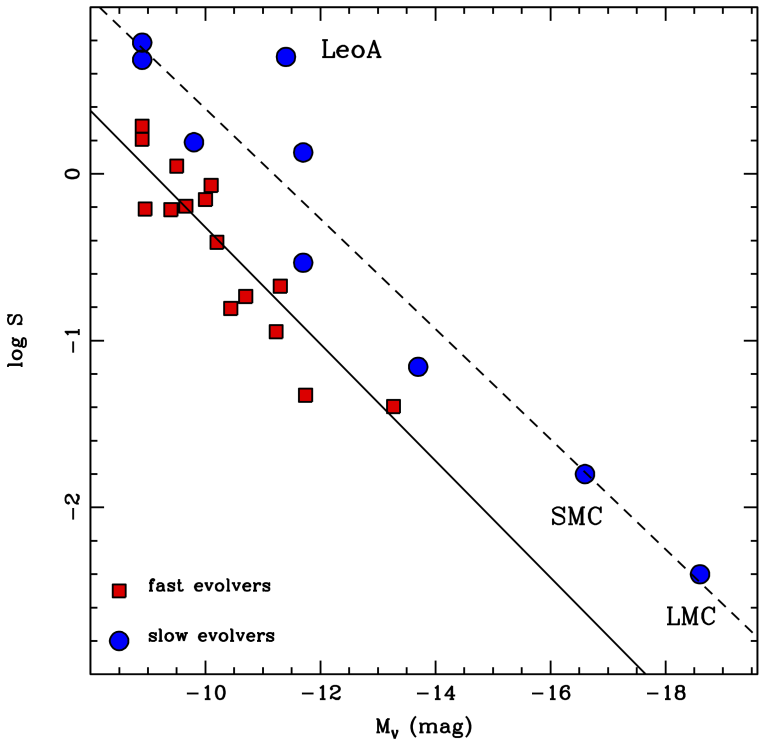

Figure 14. AC frequency (log S) per 10^5 $L_\odot$ as a function of the absolute V magnitude of the host galaxy (M_V), re-adapted from Fiorentino et al. [129]. Blue and red symbols have been used for slow and fast evolvers respectively, accordingly to the definition given by Gallart et al. [251]. The frequency of ACs is calculated from the number listed in Table 1.

5.2. Pulsation Masses for ACs

AC stars follow well-defined relations, which are the period-mass-amplitude relation (PMA) and the mass dependent period-luminosity-colour relation (PMC). In particular, it is possible to estimate individual masses once distance and reddening are known by applying the following equations, adapted from Marconi et al. [159]: The formal uncertainty on the derived masses is 5% using the PMC and 15% using the PMA (Marconi et al. [159]). It is worth mentioning that the comparison of the masses derived with a different relation is independent of the distance modulus adopted, but it does depend on the reddening correction applied. The method has been applied to the largest AC sample available, i.e., the LMC one, by Fiorentino et al. [129]. They used PMA and PMC relations to simultaneously constrain the pulsation mode and the mass of the star. This method is based on the fact that the PMA relation is only valid for the fundamental pulsator, whereas the PMC exists for both pulsation modes. Therefore, whenever the PMA and PMC for F pulsators give consistent mass, this is a robust indication that the star is actually pulsating in the fundamental mode. It is worth mentioning that the usual diagnostics used for other classes of variable stars, such as the Bailey diagram or the light curve morphology, do not allow to uniquely constrain the pulsation mode of ACs. We recall that the correct mode classification is important because it has a direct impact on the mass determination. The mean mass for ACs in the LMC has been found 1.2 ± 0.2 $M_\odot$. This method has been applied at several other galaxies: $M = 1.2 \pm 0.2$ $M_\odot$ for Leo I (Stetson et al. [60]), $M = 1.5 \pm 0.3$ $M_\odot$ for Sculptor dSph (Martínez-Vázquez et al. [47]), $M = 1.2 \pm 0.1$ $M_\odot$ Eridanus II dSph (Martínez-Vázquez et al. [54]). However, a general overview on stellar masses of ACs in all the dwarf in the LG and their possible connection with the mass of pulsating blue stragglers is still missing (Fiorentino et al. [252]). Martínez-Vázquez et al. [47] derived the pulsation mass for SX Phoenicis stars in the Sculptor dSph galaxy and found $M = 1.0 \pm 0.2$ $M_\odot$. This

suggests that the mass of these pulsating stars crossing the IS during their main sequence phase is smaller than the mass of the their evolved, brighter counterpart.

5.3. Distance

Due to the strong dependence of AC PL/Wesenheit relations from their pulsation mass, these variables cannot be safely used to set the distance of the host galaxy. Nevertheless, ACs are still important population tracers, and given the properties mentioned above they provides independent constraints to the host galaxy star formation history.

6. Discussion

6.1. Future Evolution and Challenges

The field of pulsating variable stars is now entering a new era, with new scientific and technological challenges.

ONGOING AND FUTURE SURVEYS—Large data sets from ongoing surveys allow for continuous discovery of new variable stars. Bigger surveys imply more complex data management and analysis, already well beyond the limits of the human lifetime workload capabilities. Considering the variable stars works in LG galaxies revised here, we see that most of them were small-scale, handcrafted analysis, checking candidates by eye one by one. The present and future challenges have shifted to the industrial era of automatization of the main phases of the process: identification (aiming at the highest completeness with the minimum contamination), characterization (period, amplitude, mean magnitude), and classification of variable sources. A huge effort is now required to develop analysis technique that, making use of artificial intelligence and machine learning algorithms in a big data approach, can deal with the enormous amount of incoming data (Richards et al. [253], Elorrieta et al. [254], Hernitschek et al. [255], Holl et al. [256], Hosenie et al. [257]). The best example is the Rubin-LSST which, in the near future will produce of the order of 15 Tb of data every night, and will perform real-time analysis in order to deliver alerts minutes after the observations, for prompt follow-up of varying sources.

TRACING THE MW COMPONENTS AND ITS SURROUNDINGS—Gaia DR3 will publish time series data for millions of stars over the whole sky. Combined with radial velocities and proper motions, this will allow us to identify the remnants of the MW building blocks, characterize their evolution, and associate their GCs and variable stars population so to have a complete view of the MW building blocks (Gallart et al. [251], Massari et al. [258]). Gaia's variable stars will also allow us to study at least the closest dwarf satellites, tracing their extension, internal structure, and possible interactions with the MW as traced by streams or extratidal features. In the next years, Rubin-LSST will allow us to identify RRL stars out to 400 kpc, thus including the whole MW halo and all the southern MW satellites, with 6-bands single-epoch photometry 3 magnitude fainter than, and therefore highly complementary to, Gaia. Moving to the NIR, the high spatial resolution NIR capabilities of ERIS at the VLT will be able, from 2022, to open a new path to the extremely crowded and reddened regions of the galactic bulge, helping to unravel the early history of the MW. On the other hand, wide-field space facilities such as the Nancy Grace Roman Space Telescope will allow to study RRL stars in the NIR well beyond the LG limits.

ANCHORING THE FIRST STEP OF THE DISTANCE SCALE—The improved parallaxes of Gaia will nail down the systematic errors affecting the first step of the distance scale of both Population I and Population II tracers, as discussed above. Nevertheless, Gaia information alone is not enough, as accurate metallicities for the calibrator stars are necessary. At present, a limited set of stars with accurate metallicities is available, but ongoing projects are rapidly increasing the statistics (Crestani et al. [193]). In the near future, new generation instruments such as WEAVE, which will start operating in the first half of 2022, and 4MOST, will allow to substantially increase the number of stars with accurate chemical abundance determinations, and this will be crucial to estimate the metallicity dependence of the distance relations of both RRL stars and Cepheid stars.

6.2. Homogeneity of the Data

Possibly more than most other fields in astrophysics, the variable stars studies can benefit from time series spanning over many years. This could help studying very long period variables, period changes, and pulsation mode shift among other topics. In this respect, the homogeneity of the photometry is crucial in order to exploit data from different sources.

In the present epoch, we are witnessing a change of paradigm that is not probably receiving all the attention that it should. In fact, while for decades the dominant photometric system used for variable stars has been the Johnson-Cousins one (mostly BVI), this is now changing very quickly. From one side, most large ground based telescopes are equipped with the Sloan $ugriz$ filter set, with no option to use $UBVRI$ any more. The Blanco telescope with DECam, and the Pan-Andromeda Archaeological Survey (PAndAS, McConnachie et al. [259]), which have been instrumental to discovery many low-luminosity MW and M31 satellites and their RRL stars in the last decade, are only two examples. Concerning time domain surveys, we are moving from mostly V or VI projects (e.g., OGLE, ASAS-SN) to gri, such as the ZTF which is the precursor of the Rubin-LSST, which will provide unprecedented coverage of the southern sky in the $ugrizY$ pass-bands.

If we restrict to LG dwarf galaxies, the studies on variable stars (mostly RRL stars and ACs, but also Cepheids for the MCs), we clearly identify a complex landscape:

- data for all bright MW satellites exist in BVI, and for very few, also in U (Carina, Sculptor). This is thanks to early individual works, which our group is updating thanks to a long-term project aiming at characterizing variable stars in all bright LG galaxies, exploiting the homogeneous photometry by P.B. Stetson (Stetson et al. [60], Stetson [260]);
- The low-mass MW satellites, in the so called ultra-faint regime, have been mostly studied with DECam. Among few exceptions there are some of the brightest ones, the first that were discovered, that are also visible from the northern hemisphere (Bootes IV, Dall'Ora et al. [261]; CVn I, Kuehn et al. [73]). Recently, some of the most distant MW companions have been investigate with the HST: Eridanus II ($F475W$,$F606W$,$F814W$, Martínez-Vázquez et al. [72]; and LeoT (Clementini et al. [262]; Surot et al. in prep.)
- The first variability studies in massive M31 satellites dates back to the pioneering works by Saha et al. [39], Saha and Hoessel [263], Saha et al. [264], who used g images for NGC185, NGC147 and NGC205. Moreover, early HST/WFPC2 data exist ($F450W$,$F555W$) for a few M31 satellites (Monelli et al. [36], Pritzl et al. [83,202,265]), which have been updated by more recent ACS data ($F475W$,$F814W$, Martínez-Vázquez et al. [37]). Time series for NGC 147 and NGC 185 ($F606W$,$F814W$) were published by Monelli et al. [36], while a number of fainter systems have been observed in B,V using the Large Binocular Telescope by Cusano et al. [32,35,38,84].
- Concerning more distant and isolated LG systems, we have to distinguish between studies of CC, which are bright enough to be observed from the ground (see the compilation by Tammann et al. [48]), and fainter stars such as RRL ones, which need the HST. Indeed, many galaxies between 700 kpc and 2 Mpc have published or available HST data, mostly in the $F475W$ and $F814W$ filters.

It is clear that in order to exploit all the existing data and use RRL stars in nearby galaxies *globally* to derive a general picture of the early evolution of the LG as a whole, an important homogenization effort is required (Nagarajan et al. [224]). The situation gets further complicated if we take into account Gaia, which will provide time series photometry in its native photometric system (G,B_p,R_p) for millions of variable stars in the next DR3, and the Rubin-LSST. RRL stars in all MW satellites closer than $\sim$100 kpc will be measured by Gaia (therefore Sextans, Sculptor, Carina, Ursa Minor, Draco to name a few), with full sky coverage thus beyond any existing ground-based data set. Rubin-LSST will be highly complementary, because even though restricted to the southern hemisphere, it will produce time series for object reaching r $\sim$24 mag.

While each of these existing or future data sets *per sé* will bring our knowledge of nearby galaxies a huge step forward, it will be crucial to have access to cross-matched information, exploiting multi-wavelength optical and NIR data, as well as spectroscopic information. Homogeneization of existing data on a common photometric system will be crucial to study the LG as a whole, so to allow for the use of different distance indicators (RRL stars, Cepheids, Tip of the RGB), to calibrate the distance ladder until reaching the Hubble constant.

Author Contributions: Investigation, M.M., G.F.; writing, M.M., G.F. All authors have read and agreed to the published version of the manuscript.

Funding: This research received no external funding.

Institutional Review Board Statement: Not applicable.

Informed Consent Statement: Not applicable.

Acknowledgments: The authors are in debt with Clara Martínez Vázquez and Giuseppe Bono for the support and the useful discussions. M.M. acknowledges financial support from the Spanish Ministry of Science and Innovation (MICINN) through the Spanish State Research Agency, under the grant PID2020-118778GB-I00 and the Severo Ochoa Programe 2020-2023 (CEX2019-000920-S).

Conflicts of Interest: The authors declare no conflict of interest.

Abbreviations

The following abbreviations are used in this manuscript:

AC	Anomalous Cepheids
AGB	Asymptotic Giant Branch
CC	Classical Cepheids
CMD	Colour Magnitude Diagram
dIrr	Dwarf Irregular
dSph	Dwarf Spheroidal
HB	Horizontal Branch
HST	Hubble Space Telescope
IS	Insatbility Strip
LG	Local Group
LSST	Legacy Survey of Space and Time
MW	Milky Way
NIR	Near InfraRed
PMA	Period-mass-amplitude
PMC	Period-mass-colour
RGB	Red Giant Branch
RRL	RR Lyrae
TIIC	Type II Cepheids
WEAVE	WHT Enhanced Area Velocity Explorer
ZAHB	Zero-Age Horizontal Branch
ZTF	Zwicky Transient Factory

Notes

[1] We only exclude few isolated dwarf irregular (dIrr) galaxies for which published data are typically sparse, old ground-based data for few bright Cepheids, such as WLM, Pegasus, Sextans A.

[2] The Wesenheit is pseudo-magnitude defined as the different between a magnitude in a specific passband X minus a colour term multiplied by coefficient representing the ratio between the selective absoprtion in the X band and the colour excess in the assumed colour.

[3] RRLs and CCs display different trends and different morphology of their light curves as a function of the pulsation period. A glance at the distribution of fundamental RRLs and CCs in the Bailey diagram (luminosity amplitude versus logarithmic period) shows that they follow different trends. The amplitude of fundamental RRLs strictly decreases when moving from the short- to the long-period regime (see Section 4.3), while classical Cepheids display the classical "V" shape with the secondary minimum located at the center of the Hertzsprung progression ($\sim$10 days, see also Bono et al. [104]). The difference in luminosity

amplitudes is the consequence of a stark difference in the shape of the light curves. Fundamental RRLs in the short period regime are located close to the blue (hot) edge of the IS. In this regime the RRLs attain their largest luminosity amplitudes. These RRLs have a saw-tooth light curves and also display either a dip or a change in the slope of the rising branch. These phenomena are the consequence of two different physical mechanisms:

(a) RRLs located close to the blue edge are marginally affected by convective transport. This means that the rising branch of the light curve is steep and takes place on a very short time-scale, typically of the order of 10% of the pulsation cycle. During these phases a strong shock forms and propagates. This drives several nonlinear phenomena such as the presence of hydrogen emission lines and the occurrence of helium lines both in absorption and in emission. These phenomena are not present in CCs because their variation along the pulsation cycle is smoother even in the hot side of the IS. Note that CCs are systematically cooler than RRLs, therefore, they are significantly more affected by convection than RRLs.

(b) The surface gravity of RRLs typically range from 2.5 to 3.5 dex, while for CCs typically ranges from 1.5 to 0 dex. The Ritter relations indicate that the radial displacements in CCs take place on a time scale that is, on average, at least one order of magnitude longer than in RRLs. Moreover, the range in stellar mass covered by CCs changes by at least a factor of four (from $\sim$3 to 12) while for RRLs the variation in mass is at most of the order of 30%. This means that they are significantly more uniform than CCs.

References

1. Bono, G.; Caputo, F.; Castellani, V.; Marconi, M. Nonlinear investigation of the pulsational properties of RR Lyrae variables. *Astron. Astrophys.* **1997**, *121*, 327–342. [CrossRef]
2. Marconi, M.; Coppola, G.; Bono, G.; Braga, V.; Pietrinferni, A.; Buonanno, R.; Castellani, M.; Musella, I.; Ripepi, V.; Stellingwerf, R.F. On a New Theoretical Framework for RR Lyrae Stars. I. The Metallicity Dependence. *Astrophys. J.* **2015**, *808*, 50. [CrossRef]
3. Kolenberg, K.; Szabó, R.; Kurtz, D.W.; Gilliland, R.L.; Christensen-Dalsgaard, J.; Kjeldsen, H.; Brown, T.M.; Benkő, J.M.; Chadid, M.; Derekas, A.; et al. First Kepler Results on RR Lyrae Stars. *Astrophys. J. Lett.* **2010**, *713*, L198–L203. [CrossRef]
4. Benkő, J.M.; Szabó, R. The Blazhko Effect and Additional Excited Modes in RR Lyrae Stars. *Astrophys. J. Lett.* **2015**, *809*, L19. [CrossRef]
5. Feast, M.W.; Walker, A.R. Cepheids as distance indicators. *Annu. Rev. Astron. Astrophys.* **1987**, *25*, 345–375. [CrossRef]
6. Riess, A.G.; Casertano, S.; Yuan, W.; Bowers, J.B.; Macri, L.; Zinn, J.C.; Scolnic, D. Cosmic Distances Calibrated to 1% Precision with Gaia EDR3 Parallaxes and Hubble Space Telescope Photometry of 75 Milky Way Cepheids Confirm Tension with ΛCDM. *Astrophys. J. Lett.* **2021**, *908*, L6. [CrossRef]
7. De Somma, G.; Marconi, M.; Cassisi, S.; Ripepi, V.; Leccia, S.; Molinaro, R.; Musella, I. Updated theoretical period-age and period-age-colour relations for Galactic Classical Cepheids: An application to the Gaia DR2 sample. *Mon. Not. R. Astron. Soc.* **2020**, *496*, 5039–5051. [CrossRef]
8. Martínez-Vázquez, C.E.; Monelli, M.; Gallart, C.; Bono, G.; Bernard, E.J.; Stetson, P.B.; Ferraro, I.; Walker, A.R.; Dall'Ora, M.; Fiorentino, G.; et al. Probing the early chemical evolution of the Sculptor dSph with purely old stellar tracers. *Mon. Not. R. Astron. Soc.* **2016**, *461*, L41–L45. [CrossRef]
9. Tolstoy, E.; Hill, V.; Tosi, M. Star-Formation Histories, Abundances, and Kinematics of Dwarf Galaxies in the Local Group. *Annu. Rev. Astron. Astrophys.* **2009**, *47*, 371–425. [CrossRef]
10. Dekel, A.; Silk, J. The Origin of Dwarf Galaxies, Cold Dark Matter, and Biased Galaxy Formation. *Astrophys. J.* **1986**, *303*, 39. [CrossRef]
11. Sawala, T.; Scannapieco, C.; Maio, U.; White, S. Formation of isolated dwarf galaxies with feedback. *Mon. Not. R. Astron. Soc.* **2010**, *402*, 1599–1613. [CrossRef]
12. Mayer, L.; Governato, F.; Colpi, M.; Moore, B.; Quinn, T.; Wadsley, J.; Stadel, J.; Lake, G. The Metamorphosis of Tidally Stirred Dwarf Galaxies. *Astrophys. J.* **2001**, *559*, 754–784. [CrossRef]
13. Gallart, C.; Zoccali, M.; Aparicio, A. The Adequacy of Stellar Evolution Models for the Interpretation of the Color-Magnitude Diagrams of Resolved Stellar Populations. *Annu. Rev. Astron. Astrophys.* **2005**, *43*, 387–434. [CrossRef]
14. Bono, G.; Caputo, F.; Santolamazza, P. Evolutionary scenario for metal-poor pulsating stars. I. Type II Cepheids. *Astron. Astrophys.* **1997**, *317*, 171–177.
15. Bono, G.; Braga, V.F.; Fiorentino, G.; Salaris, M.; Pietrinferni, A.; Castellani, M.; Di Criscienzo, M.; Fabrizio, M.; Martínez-Vázquez, C.E.; Monelli, M. Evolutionary and pulsation properties of Type II Cepheids. *Astron. Astrophys.* **2020**, *644*, A96. [CrossRef]
16. Udalski, A.; Szymanski, M.; Kaluzny, J.; Kubiak, M.; Mateo, M. The Optical Gravitational Lensing Experiment. *Acta Astron.* **1992**, *42*, 253–284.
17. Zinn, R.; Horowitz, B.; Vivas, A.K.; Baltay, C.; Ellman, N.; Hadjiyska, E.; Rabinowitz, D.; Miller, L. La Silla QUEST RR Lyrae Star Survey: Region I. *Astrophys. J.* **2014**, *781*, 22. [CrossRef]
18. Woźniak, P.R.; Vestrand, W.T.; Akerlof, C.W.; Balsano, R.; Bloch, J.; Casperson, D.; Fletcher, S.; Gisler, G.; Kehoe, R.; Kinemuchi, K.; et al. Northern Sky Variability Survey: Public Data Release. *Astron. J.* **2004**, *127*, 2436–2449. [CrossRef]
19. Szczygieł, D.M.; Pojmański, G.; Pilecki, B. Galactic Fundamental Mode RR˜Lyrae Stars. Period-Amplitude Diagram, Metallicities and Distribution. *Acta Astron.* **2009**, *59*, 137–167.
20. Drake, A.J.; Catelan, M.; Djorgovski, S.G.; Torrealba, G.; Graham, M.J.; Belokurov, V.; Koposov, S.E.; Mahabal, A.; Prieto, J.L.; Donalek, C.; et al. Probing the Outer Galactic Halo with RR Lyrae from the Catalina Surveys. *Astrophys. J.* **2013**, *763*, 32. [CrossRef]

21. Cioni, M.R.L.; Clementini, G.; Girardi, L.; Guandalini, R.; Gullieuszik, M.; Miszalski, B.; Moretti, M.I.; Ripepi, V.; Rubele, S.; Bagheri, G.; et al. The VMC survey. I. Strategy and first data. *Astron. Astrophys.* **2011**, *527*, A116. [CrossRef]
22. Minniti, D.; Lucas, P.W.; Emerson, J.P.; Saito, R.K.; Hempel, M.; Pietrukowicz, P.; Ahumada, A.V.; Alonso, M.V.; Alonso-Garcia, J.; Arias, J.I.; et al. VISTA Variables in the Via Lactea (VVV): The public ESO near-IR variability survey of the Milky Way. *New Astron.* **2010**, *15*, 433–443. [CrossRef]
23. Wright, E.L.; Eisenhardt, P.R.M.; Mainzer, A.K.; Ressler, M.E.; Cutri, R.M.; Jarrett, T.; Kirkpatrick, J.D.; Padgett, D.; McMillan, R.S.; Skrutskie, M.; et al. The Wide-field Infrared Survey Explorer (WISE): Mission Description and Initial On-orbit Performance. *Astron. J.* **2010**, *140*, 1868–1881. [CrossRef]
24. Chambers, K.C.; Magnier, E.A.; Metcalfe, N.; Flewelling, H.A.; Huber, M.E.; Waters, C.Z.; Denneau, L.; Draper, P.W.; Farrow, D.; Finkbeiner, D.P.; et al. The Pan-STARRS1 Surveys. *arXiv* **2016**, arXiv:astro-ph.IM/1612.05560.
25. Masci, F.J.; Laher, R.R.; Rusholme, B.; Shupe, D.L.; Groom, S.; Surace, J.; Jackson, E.; Monkewitz, S.; Beck, R.; Flynn, D.; et al. The Zwicky Transient Facility: Data Processing, Products, and Archive. *Publ. Astron. Soc. Pac.* **2019**, *131*, 018003. [CrossRef]
26. Bellm, E.C.; Kulkarni, S.R.; Graham, M.J.; Dekany, R.; Smith, R.M.; Riddle, R.; Masci, F.J.; Helou, G.; Prince, T.A.; Adams, S.M.; et al. The Zwicky Transient Facility: System Overview, Performance, and First Results. *Publ. Astron. Soc. Pac.* **2019**, *131*, 018002. [CrossRef]
27. Ivezić, Ž.; Kahn, S.M.; Tyson, J.A.; Abel, B.; Acosta, E.; Allsman, R.; Alonso, D.; AlSayyad, Y.; Anderson, S.F.; Andrew, J.; et al. LSST: From Science Drivers to Reference Design and Anticipated Data Products. *Astrophys. J.* **2019**, *873*, 111. [CrossRef]
28. Soszyński, I.; Udalski, A.; Szymański, M.K.; Kubiak, M.; Pietrzyński, G.; Wyrzykowski, Ł.; Szewczyk, O.; Ulaczyk, K.; Poleski, R. The Optical Gravitational Lensing Experiment. The OGLE-III Catalog of Variable Stars. III. RR Lyrae Stars in the Large Magellanic Cloud. *Acta Astron.* **2009**, *59*, 1–18.
29. Soszyński, I.; Poleski, R.; Udalski, A.; Szymanski, M.K.; Kubiak, M.; Pietrzynski, G.; Wyrzykowski, L.; Szewczyk, O.; Ulaczyk, K. The Optical Gravitational Lensing Experiment. The OGLE-III Catalog of Variable Stars. I. Classical Cepheids in the Large Magellanic Cloud. *Acta Astron.* **2008**, *58*, 163–185.
30. Soszyński, I.; Udalski, A.; Szymański, M.K.; Kubiak, M.; Pietrzyński, G.; Wyrzykowski, Ł.; Szewczyk, O.; Ulaczyk, K.; Poleski, R. The Optical Gravitational Lensing Experiment. The OGLE-III Catalog of Variable Stars. II. Type II Cepheids and Anomalous Cepheids in the Large Magellanic Cloud. *Acta Astron.* **2008**, *58*, 293.
31. Yang, S.C.; Wagner-Kaiser, R.; Sarajedini, A.; Kim, S.C.; Kyeong, J. The Early Chemical Enrichment Histories of Two Sculptor Group Dwarf Galaxies as Revealed by RR Lyrae Variables. *Astrophys. J.* **2014**, *784*, 76. [CrossRef]
32. Cusano, F.; Clementini, G.; Garofalo, A.; Cignoni, M.; Federici, L.; Marconi, M.; Musella, I.; Ripepi, V.; Boutsia, K.; Fumana, M.; et al. Dwarf Spheroidal Satellites of M31. I. Variable Stars and Stellar Populations in Andromeda XIX. *Astrophys. J.* **2013**, *779*, 7. [CrossRef]
33. Bernard, E.J.; Monelli, M.; Gallart, C.; Aparicio, A.; Cassisi, S.; Drozdovsky, I.; Hidalgo, S.L.; Skillman, E.D.; Stetson, P.B. The ACS LCID Project. II. Faint Variable Stars in the Isolated Dwarf Irregular Galaxy IC 1613. *Astrophys. J.* **2010**, *712*, 1259–1276. [CrossRef]
34. Monelli, M.; Bernard, E.J.; Gallart, C.; Fiorentino, G.; Drozdovsky, I.; Aparicio, A.; Bono, G.; Cassisi, S.; Skillman, E.D.; Stetson, P.B. Variable stars in the Cetus dwarf spheroidal galaxy: Population gradients and connections with the star formation history. *Mon. Not. R. Astron. Soc.* **2012**, *422*, 89–105. [CrossRef]
35. Cusano, F.; Garofalo, A.; Clementini, G.; Cignoni, M.; Federici, L.; Marconi, M.; Ripepi, V.; Musella, I.; Testa, V.; Carini, R.; et al. Variable Stars and Stellar Populations in Andromeda XXV. III. A Central Cluster or the Galaxy Nucleus? *Astrophys. J.* **2016**, *829*, 26. [CrossRef]
36. Monelli, M.; Fiorentino, G.; Bernard, E.J.; Martínez-Vázquez, C.E.; Bono, G.; Gallart, C.; Dall'Ora, M.; Stetson, P.B. Variable Stars in Local Group Galaxies. III. And VII, NGC 147, and NGC 185: Insight into the Building Blocks of the M31 Halo. *Astrophys. J.* **2017**, *842*, 60. [CrossRef]
37. Martínez-Vázquez, C.E.; Monelli, M.; Bernard, E.J.; Gallart, C.; Stetson, P.B.; Skillman, E.D.; Bono, G.; Cassisi, S.; Fiorentino, G.; McQuinn, K.B.W.; et al. The ISLAnds Project. III. Variable Stars in Six Andromeda Dwarf Spheroidal Galaxies. *Astrophys. J.* **2017**, *850*, 137. [CrossRef]
38. Cusano, F.; Garofalo, A.; Clementini, G.; Cignoni, M.; Muraveva, T.; Tessicini, G.; Testa, V.; Paris, D.; Federici, L.; Marconi, M.; et al. Variable Stars and Stellar Populations in Andromeda XXVII. IV. An Off-centered, Disrupted Galaxy. *Astrophys. J.* **2017**, *851*, 9. [CrossRef]
39. Saha, A.; Hoessel, J.G.; Krist, J. RR Lyrae Stars in Local Group Galaxies. III. NGC 205. *Astron. J.* **1992**, *103*, 84. [CrossRef]
40. Fiorentino, G.; Clementini, G.; Marconi, M.; Musella, I.; Saha, A.; Tosi, M.; Contreras Ramos, R.; Annibali, F.; Aloisi, A.; van der Marel, R. Ultra long period Cepheids: A primary standard candle out to the Hubble flow. *Astrophys. Space Sci.* **2012**, *341*, 143–150. [CrossRef]
41. Sarajedini, A.; Yang, S.C.; Monachesi, A.; Lauer, T.R.; Trager, S.C. An ancient metal-poor population in M32, and halo satellite accretion in M31, identified by RR Lyrae stars. *Mon. Not. R. Astron. Soc.* **2012**, *425*, 1459–1472. [CrossRef]
42. Yang, S.C.; Sarajedini, A. HST/WFPC2 imaging of the dwarf satellites And XI and And XIII: horizontal branch morphology and RR Lyraes. *Mon. Not. R. Astron. Soc.* **2012**, *419*, 1362–1375. [CrossRef]
43. Soszyński, I.; Udalski, A.; Szymański, M.K.; Pietrzyński, G.; Wyrzykowski, Ł.; Ulaczyk, K.; Poleski, R.; Pietrukowicz, P.; Kozłowski, S.; Skowron, J.; et al. The OGLE Collection of Variable Stars. Anomalous Cepheids in the Magellanic Clouds. *Acta Astron.* **2015**, *65*, 233–250.

44. Soszyński, I.; Udalski, A.; Szymański, M.K.; Wyrzykowski, Ł.; Ulaczyk, K.; Poleski, R.; Pietrukowicz, P.; Kozłowski, S.; Skowron, D.M.; Skowron, J.; et al. The OGLE Collection of Variable Stars. Over 45,000 RR Lyrae Stars in the Magellanic System. *Acta Astron.* **2016**, *66*, 131–147.
45. Soszyński, I.; Udalski, A.; Szymański, M.K.; Wyrzykowski, Ł.; Ulaczyk, K.; Poleski, R.; Pietrukowicz, P.; Kozłowski, S.; Skowron, D.; Skowron, J.; et al. The OGLE Collection of Variable Stars. Type II Cepheids in the Magellanic System. *Acta Astron.* **2018**, *68*, 89–109. [CrossRef]
46. Monelli, M.; Martínez-Vázquez, C.E.; Bernard, E.J.; Gallart, C.; Skillman, E.D.; Weisz, D.R.; Dolphin, A.E.; Hidalgo, S.L.; Cole, A.A.; Martin, N.F.; et al. The ISLANDS Project. I. Andromeda XVI, An Extremely Low Mass Galaxy Not Quenched by Reionization. *Astrophys. J.* **2016**, *819*, 147. [CrossRef]
47. Martínez-Vázquez, C.E.; Stetson, P.B.; Monelli, M.; Bernard, E.J.; Fiorentino, G.; Gallart, C.; Bono, G.; Cassisi, S.; Dall'Ora, M.; Ferraro, I.; et al. Variable stars in Local Group Galaxies—II. Sculptor dSph. *Mon. Not. R. Astron. Soc.* **2016**, *462*, 4349–4370. [CrossRef]
48. Tammann, G.A.; Reindl, B.; Sandage, A. New period-luminosity and period-color relations of classical Cepheids. IV. The low-metallicity galaxies IC 1613, WLM, Pegasus, Sextans A and B, and Leo A in comparison to SMC. *Astron. Astrophys.* **2011**, *531*, A134. [CrossRef]
49. Tanakul, N.; Yang, S.C.; Sarajedini, A. RR Lyrae variables in M33: Two new fields and an analysis of the galaxy's population. *Mon. Not. R. Astron. Soc.* **2017**, *468*, 870–884. [CrossRef]
50. Gallart, C.; Aparicio, A.; Freedman, W.L.; Madore, B.F.; Martínez-Delgado, D.; Stetson, P.B. The Variable-Star Population in Phoenix: Coexistence of Anomalous and Short-Period Classical Cepheids and Detection of RR Lyrae Variables. *Astron. J.* **2004**, *127*, 1486–1501. [CrossRef]
51. Ordoñez, A.J.; Yang, S.C.; Sarajedini, A. The RR Lyrae Variable Population in the Phoenix Dwarf Galaxy. *Astrophys. J.* **2014**, *786*, 147. [CrossRef]
52. Boettcher, E.; Willman, B.; Fadely, R.; Strader, J.; Baker, M.; Hopkins, E.; Tasnim Ananna, T.; Cunningham, E.C.; Douglas, T.; Gilbert, J.; et al. A Search for RR Lyrae Stars in Segue 2 and Segue 3. *Astron. J.* **2013**, *146*, 94. [CrossRef]
53. Vivas, A.K.; Martínez-Vázquez, C.; Walker, A.R. Gaia RR Lyrae Stars in Nearby Ultra-faint Dwarf Satellite Galaxies. *Astrophys. J.* **2020**, *247*, 35. [CrossRef]
54. Martínez-Vázquez, C.E.; Monelli, M.; Cassisi, S.; Taibi, S.; Gallart, C.; Vivas, A.K.; Walker, A.R.; Martín-Ravelo, P.; Zenteno, A.; Battaglia, G.; et al. Variable stars in Local Group galaxies—V. The fast and early evolution of the low-mass Eridanus II dSph galaxy. *Mon. Not. R. Astron. Soc.* **2021**, *508*, 1064–1083. [CrossRef]
55. Coppola, G.; Marconi, M.; Stetson, P.B.; Bono, G.; Braga, V.F.; Ripepi, V.; Dall'Ora, M.; Musella, I.; Buonanno, R.; Fabrizio, M.; et al. The Carina Project IX: On Hydrogen and Helium Burning Variables. *Astrophys. J.* **2015**, *814*, 71. [CrossRef]
56. Neeley, J.R.; Monelli, M.; Marengo, M.; Fiorentino, G.; Vivas, A.K.; Walker, A.; Gallart, C.; Martínez-Vázquez, C.E.; Bono, G.; Cassisi, S.; et al. Variable Stars in Local Group Galaxies. VI. The Isolated Dwarfs VV 124 and KKr 25. *Astrophys. J.* **2021**, *920*, 152. [CrossRef]
57. Vivas, A.K.; Martínez-Vázquez, C.E.; Walker, A.R.; Belokurov, V.; Li, T.S.; Erkal, D. Variable Stars in the Giant Satellite Galaxy Antlia 2. *Astrophys. J.* **2022**, *926*, 78. [CrossRef]
58. Bernard, E.J.; Monelli, M.; Gallart, C.; Fiorentino, G.; Cassisi, S.; Aparicio, A.; Cole, A.A.; Drozdovsky, I.; Hidalgo, S.L.; Skillman, E.D.; et al. The ACS LCID Project - VIII. The short-period Cepheids of Leo A. *Mon. Not. R. Astron. Soc.* **2013**, *432*, 3047–3061. [CrossRef]
59. Simon, J.D.; Geha, M.; Minor, Q.E.; Martinez, G.D.; Kirby, E.N.; Bullock, J.S.; Kaplinghat, M.; Strigari, L.E.; Willman, B.; Choi, P.I.; et al. A Complete Spectroscopic Survey of the Milky Way Satellite Segue 1: The Darkest Galaxy. *Astrophys. J.* **2011**, *733*, 46. [CrossRef]
60. Stetson, P.B.; Fiorentino, G.; Bono, G.; Bernard, E.J.; Monelli, M.; Iannicola, G.; Gallart, C.; Ferraro, I. Homogeneous Photometry VI: Variable Stars in the Leo I Dwarf Spheroidal Galaxy. *Publ. Astron. Soc. Pac.* **2014**, *126*, 616–641. [CrossRef]
61. Mateo, M.; Fischer, P.; Krzeminski, W. Variable Stars in the Sextans Dwarf Spheroidal Galaxy. *Astron. J.* **1995**, *110*, 2166. [CrossRef]
62. Amigo, P.; Stetson, P.B.; Catelan, M.; Zoccali, M.; Smith, H.A. Time-series BVI Photometry for the Globular Cluster NGC 6981. *Astron. J.* **2013**, *146*, 130. [CrossRef]
63. Vivas, A.K.; Alonso-García, J.; Mateo, M.; Walker, A.; Howard, B. The Population of Pulsating Variable Stars in the Sextans Dwarf Spheroidal Galaxy. *Astron. J.* **2019**, *157*, 35. [CrossRef]
64. McQuinn, K.B.W.; Skillman, E.D.; Dolphin, A.; Cannon, J.M.; Salzer, J.J.; Rhode, K.L.; Adams, E.A.K.; Berg, D.; Giovanelli, R.; Girardi, L.; et al. Leo P: An Unquenched Very Low-mass Galaxy. *Astrophys. J.* **2015**, *812*, 158. [CrossRef]
65. Siegel, M.H.; Majewski, S.R. Exploring the Leo II Dwarf Spheroidal Galaxy. I. The Variable Star Content. *Astron. J.* **2000**, *120*, 284–297. [CrossRef]
66. Medina, G.E.; Muñoz, R.R.; Vivas, A.K.; Förster, F.; Carlin, J.L.; Martinez, J.; Galbany, L.; González-Gaitán, S.; Hamuy, M.; de Jaeger, T.; et al. Serendipitous Discovery of RR Lyrae Stars in the Leo V Ultra-faint Galaxy. *Astrophys. J. Lett.* **2017**, *845*, L10. [CrossRef]
67. Moretti, A.; Piotto, G.; Arcidiacono, C.; Milone, A.P.; Ragazzoni, R.; Falomo, R.; Farinato, J.; Bedin, L.R.; Anderson, J.; Sarajedini, A.; et al. MCAO near-IR photometry of the globular cluster NGC 6388: MAD observations in crowded fields. *Astron. Astrophys.* **2009**, *493*, 539–546. [CrossRef]

68. Joo, S.J.; Kyeong, J.; Yang, S.C.; Han, S.I.; Sung, E.C.; Kim, D.; Jeong, H.; Ree, C.H.; Rey, S.C.; Jerjen, H.; et al. RR Lyrae Variables in the Crater II Dwarf Galaxy. *Astrophys. J.* **2018**, *861*, 23. [CrossRef]
69. Monelli, M.; Walker, A.R.; Martínez-Vázquez, C.E.; Stetson, P.B.; Gallart, C.; Bernard, E.J.; Bono, G.; Vivas, A.K.; Andreuzzi, G.; Dall'Ora, M.; et al. Variable stars in local group galaxies—IV. RR Lyrae stars in the central regions of the low-density galaxy Crater II. *Mon. Not. R. Astron. Soc.* **2018**, *479*, 4279–4291. [CrossRef]
70. Vivas, A.K.; Walker, A.R.; Martínez-Vázquez, C.E.; Monelli, M.; Bono, G.; Dorta, A.; Nidever, D.L.; Fiorentino, G.; Gallart, C.; Andreuzzi, G.; et al. A DECam view of the diffuse dwarf galaxy Crater II—Variable stars. *Mon. Not. R. Astron. Soc.* **2020**, *492*, 1061–1077. [CrossRef]
71. Vivas, A.K.; Olsen, K.; Blum, R.; Nidever, D.L.; Walker, A.R.; Martin, N.F.; Besla, G.; Gallart, C.; van der Marel, R.P.; Majewski, S.R.; et al. Variable Stars in the Field of the Hydra II Ultra-faint Dwarf Galaxy. *Astron. J.* **2016**, *151*, 118. [CrossRef]
72. Martínez-Vázquez, C.E.; Cerny, W.; Vivas, A.K.; Drlica-Wagner, A.; Pace, A.B.; Simon, J.D.; Munoz, R.R.; Walker, A.R.; Allam, S.; Tucker, D.L.; et al. RR Lyrae Stars in the Newly Discovered Ultra-faint Dwarf Galaxy Centaurus I. *Astron. J.* **2021**, *162*, 253. [CrossRef]
73. Kuehn, C.; Kinemuchi, K.; Ripepi, V.; Clementini, G.; Dall'Ora, M.; Di Fabrizio, L.; Rodgers, C.T.; Greco, C.; Marconi, M.; Musella, I.; et al. Variable Stars in the Newly Discovered Milky Way Dwarf Spheroidal Satellite Canes Venatici I. *Astrophys. J. Lett.* **2008**, *674*, L81–L84. [CrossRef]
74. Nemec, J.M.; Wehlau, A.; Mendes de Oliveira, C. Variable stars in the Ursa Minor dwarf galaxy. *Astron. J.* **1988**, *96*, 528–559. [CrossRef]
75. Musella, I.; Ripepi, V.; Marconi, M.; Clementini, G.; Dall'Ora, M.; Scowcroft, V.; Moretti, M.I.; Di Fabrizio, L.; Greco, C.; Coppola, G.; et al. Stellar Archeology in the Galactic Halo with Ultra-faint Dwarfs. VII. Hercules. *Astrophys. J.* **2012**, *756*, 121. [CrossRef]
76. Kinemuchi, K.; Harris, H.C.; Smith, H.A.; Silbermann, N.A.; Snyder, L.A.; La Cluyzé, A.P.; Clark, C.L. The Variable Stars of the Draco Dwarf Spheroidal Galaxy: Revisited. *Astron. J.* **2008**, *136*, 1921–1939. [CrossRef]
77. Soszyński, I.; Udalski, A.; Szymański, M.K.; Pietrukowicz, P.; Mróz, P.; Skowron, J.; Kozłowski, S.; Poleski, R.; Skowron, D.; Pietrzyński, G.; et al. Over 38000 RR Lyrae Stars in the OGLE Galactic Bulge Fields. *Acta Astron.* **2014**, *64*, 177–196.
78. Hamanowicz, A.; Pietrukowicz, P.; Udalski, A.; Mróz, P.; Soszyński, I.; Szymański, M.K.; Skowron, J.; Poleski, R.; Wyrzykowski, Ł.; Kozłowski, S.; et al. OGLE Study of the Sagittarius Dwarf Spheroidal Galaxy and its M54 Globular Cluster. *Acta Astron.* **2016**, *66*, 197–217.
79. Baldacci, L.; Rizzi, L.; Clementini, G.; Held, E.V. Variable stars in the dwarf irregular galaxy NGC 6822: Thephotometric catalogue. *Astron. Astrophys.* **2005**, *431*, 1189–1201. [CrossRef]
80. Martínez-Vázquez, C.E.; Vivas, A.K.; Gurevich, M.; Walker, A.R.; McCarthy, M.; Pace, A.B.; Stringer, K.M.; Santiago, B.; Hounsell, R.; Macri, L.; et al. Search for RR Lyrae stars in DES ultrafaint systems: Grus I, Kim 2, Phoenix II, and Grus II. *Mon. Not. R. Astron. Soc.* **2019**, *490*, 2183–2199. [CrossRef]
81. Garofalo, A.; Tantalo, M.; Cusano, F.; Clementini, G.; Calura, F.; Muraveva, T.; Paris, D.; Speziali, R. Born in a Pair (?): Pisces II and Pegasus III. *Astrophys. J.* **2021**, *916*, 10. [CrossRef]
82. Bernard, E.J.; Monelli, M.; Gallart, C.; Drozdovsky, I.; Stetson, P.B.; Aparicio, A.; Cassisi, S.; Mayer, L.; Cole, A.A.; Hidalgo, S.L.; et al. The ACS LCID Project. I. Short-Period Variables in the Isolated Dwarf Spheroidal Galaxies Cetus and Tucana. *Astrophys. J.* **2009**, *699*, 1742–1764. [CrossRef]
83. Pritzl, B.J.; Armandroff, T.E.; Jacoby, G.H.; Da Costa, G.S. The Dwarf Spheroidal Companions to M31: Variable Stars in Andromeda VI. *Astron. J.* **2002**, *124*, 1464–1485. [CrossRef]
84. Cusano, F.; Garofalo, A.; Clementini, G.; Cignoni, M.; Federici, L.; Marconi, M.; Musella, I.; Ripepi, V.; Speziali, R.; Sani, E.; et al. Variable Stars and Stellar Populations in Andromeda XXI. II. Another Merged Galaxy Satellite of M31? *Astrophys. J.* **2015**, *806*, 200. [CrossRef]
85. Walker, A.R. CCD photometry of the RR Lyrae variables in the LMC cluster NGC 2257 and the adjacent field. *Astron. J.* **1989**, *98*, 2086–2123. [CrossRef]
86. Braga, V.F.; Crestani, J.; Fabrizio, M.; Bono, G.; Sneden, C.; Preston, G.W.; Storm, J.; Kamann, S.; Latour, M.; Lala, H.; et al. On the Use of Field RR Lyrae as Galactic Probes. V. Optical and Radial Velocity Curve Templates. *Astrophys. J.* **2021**, *919*, 85. [CrossRef]
87. Beaton, R.L.; Freedman, W.L.; Madore, B.F.; Bono, G.; Carlson, E.K.; Clementini, G.; Durbin, M.J.; Garofalo, A.; Hatt, D.; Jang, I.S.; et al. The Carnegie-Chicago Hubble Program. I. An Independent Approach to the Extragalactic Distance Scale Using Only Population II Distance Indicators. *Astrophys. J.* **2016**, *832*, 210. [CrossRef]
88. Baade, W.; Hubble, E. The New Stellar Systems in Sculptor and Fornax. *Publ. Astron. Soc. Pac.* **1939**, *51*, 40. [CrossRef]
89. Thackeray, A.D. Variables in the Sculptor system. *Observatory* **1950**, *70*, 144–146.
90. Thackeray, A.D. 1951 November 9 meeting of the Royal Astronomical Society. *Observatory* **1951**, *71*, 219–228.
91. Thackeray, A.D.; Wesselink, A.J. Distances of the Magellanic Clouds. *New Astron.* **1953**, *171*, 693. [CrossRef]
92. Thackeray, A.D. Periods and light-curves of variable stars in NGC 121. *Mon. Not. R. Astron. Soc.* **1958**, *118*, 117. [CrossRef]
93. Alexander, J.B. Variable stars in NGC 2257. *Mon. Not. R. Astron. Soc.* **1960**, *121*, 97. [CrossRef]
94. Baade, W.; Swope, H.H. The Draco system, a dwarf galaxy. *Astron. J.* **1961**, *66*, 300–347. [CrossRef]
95. van Agt, S.L.T.J. A discussion of the Ursa Minor dwarf galaxy based on plates obtained by Walter Baade. *Bull. Astron. Inst. Neth.* **1967**, *19*, 275.
96. Swope, H.H. Progress Report on the Leo II System. *Publ. Astron. Soc. Pac.* **1967**, *79*, 439. [CrossRef]

97. van Agt, S.L.T.J. Magnitudes, phases and light-curves of variable stars in the central region of the Ursa Minor dwarf galaxy. *Bull. Astron. Inst. Neth. Suppl. Ser.* **1968**, *2*, 237.
98. Hodge, P.W.; Wright, F.W. Variable stars in the Leo I dwarf galaxy. *Astron. J.* **1978**, *83*, 228–233. [CrossRef]
99. Bersier, D.; Wood, P.R. Variable Stars in the Fornax Dwarf Galaxy. *Astron. J.* **2002**, *123*, 840–847. [CrossRef]
100. Dall'Ora, M.; Ripepi, V.; Caputo, F.; Castellani, V.; Bono, G.; Smith, H.A.; Brocato, E.; Buonanno, R.; Castellani, M.; Corsi, C.E.; et al. The Carina Project. I. Bright Variable Stars. *Astron. J.* **2003**, *126*, 197–217. [CrossRef]
101. Alcock, C.; Allsman, R.A.; Axelrod, T.S.; Bennett, D.P.; Cook, K.H.; Freeman, K.C.; Griest, K.; Marshall, S.L.; Peterson, B.A.; Pratt, M.R.; et al. The MACHO Project LMC Variable Star Inventory.II.LMC RR Lyrae Stars- Pulsational Characteristics and Indications of a Global Youth of the LMC. *Astron. J.* **1996**, *111*, 1146. [CrossRef]
102. Soszyński, I.; Smolec, R.; Udalski, A.; Pietrukowicz, P. Type II Cepheids Pulsating in the First Overtone from the OGLE Survey. *Astrophys. J.* **2019**, *873*, 43. [CrossRef]
103. Da Costa, G.S.; Rejkuba, M.; Jerjen, H.; Grebel, E.K. Ancient Stars Beyond the Local Group: RR Lyrae Variables and Blue Horizontal Branch Stars in Sculptor Group Dwarf Galaxies. *Astrophys. J. Lett.* **2010**, *708*, L121–L125. [CrossRef]
104. Bono, G.; Marconi, M.; Stellingwerf, R.F. Classical Cepheid pulsation models—VI. The Hertzsprung progression. *Astron. Astrophys.* **2000**, *360*, 245–262.
105. Bono, G.; Caputo, F.; Marconi, M. On the second-overtone stability among Small Magellanic Cloud Cepheids. *Mon. Not. R. Astron. Soc.* **2001**, *325*, 1353–1358. [CrossRef]
106. Leavitt, H.S.; Pickering, E.C. Periods of 25 Variable Stars in the Small Magellanic Cloud. *Harv. Coll. Obs. Circ.* **1912**, *173*, 1–3.
107. Riess, A.G.; Fliri, J.; Valls-Gabaud, D. Cepheid Period-Luminosity Relations in the Near-infrared and the Distance to M31 from the Hubble Space Telescope Wide Field Camera 3. *Astrophys. J.* **2012**, *745*, 156. [CrossRef]
108. Riess, A.G.; Rodney, S.A.; Scolnic, D.M.; Shafer, D.L.; Strolger, L.G.; Ferguson, H.C.; Postman, M.; Graur, O.; Maoz, D.; Jha, S.W.; et al. Type Ia Supernova Distances at z gt 1.5 from the Hubble Space Telescope Multi-Cycle Treasury Programs: The Early Expansion Rate. *arXiv* **2017**, arXiv:1710.00844.
109. Fiorentino, G.; Caputo, F.; Marconi, M.; Musella, I. Theoretical Models for Classical Cepheids. VIII. Effects of Helium and Heavy-Element Abundance on the Cepheid Distance Scale. *Astrophys. J.* **2002**, *576*, 402–412. [CrossRef]
110. Marconi, M.; Musella, I.; Fiorentino, G. Cepheid Pulsation Models at Varying Metallicity and $\Delta Y/\Delta Z$. *Astrophys. J.* **2005**, *632*, 590–610. [CrossRef]
111. Macri, L.M.; Stanek, K.Z.; Bersier, D.; Greenhill, L.J.; Reid, M.J. A New Cepheid Distance to the Maser-Host Galaxy NGC 4258 and Its Implications for the Hubble Constant. *Astrophys. J.* **2006**, *652*, 1133–1149. [CrossRef]
112. Fiorentino, G.; Musella, I.; Marconi, M. Cepheid theoretical models and observations in HST/WFC3 filters: The effect on the Hubble constant H_0. *Mon. Not. R. Astron. Soc.* **2013**, *434*, 2866–2876. [CrossRef]
113. Ripepi, V.; Catanzaro, G.; Molinaro, R.; Gatto, M.; De Somma, G.; Marconi, M.; Romaniello, M.; Leccia, S.; Musella, I.; Trentin, E.; et al. Cepheid metallicity in the Leavitt law (C-metall) survey—I. HARPS-N@TNG spectroscopy of 47 classical Cepheids and 1 BL Her variables. *Mon. Not. R. Astron. Soc.* **2021**, *508*, 4047–4071. [CrossRef]
114. Breuval, L.; Kervella, P.; Wielgórski, P.; Gieren, W.; Graczyk, D.; Trahin, B.; Pietrzyński, G.; Arenou, F.; Javanmardi, B.; Zgirski, B. The Influence of Metallicity on the Leavitt Law from Geometrical Distances of Milky Way and Magellanic Cloud Cepheids. *Astrophys. J.* **2021**, *913*, 38. [CrossRef]
115. Marconi, M.; Bono, G.; Caputo, F.; Cassisi, S.; Pietrukowicz, P.; Pietrzynski, G.; Gieren, W. Classical Cepheids as age indicators. *Mem. Della Soc. Astron. Ital.* **2006**, *77*, 67.
116. Macri, L. The role of the LMC in the Extragalactic Distance Scale: Cepheids and Miras. In Proceedings of the A Synoptic View of the Magellanic Clouds: VMC, Gaia and Beyond, Garching, Germany, 9–13 September 2019; p. 42. [CrossRef]
117. Soszyński, I.; Poleski, R.; Udalski, A.; Szymański, M.K.; Kubiak, M.; Pietrzyński, G.; Wyrzykowski, Ł.; Szewczyk, O.; Ulaczyk, K. The Optical Gravitational Lensing Experiment. The OGLE-III Catalog of Variable Stars. VII. Classical Cepheids in the Small Magellanic Cloud. *Acta Astron.* **2010**, *60*, 17–39.
118. Gieren, W.; Górski, M.; Pietrzyński, G.; Konorski, P.; Suchomska, K.; Graczyk, D.; Pilecki, B.; Bresolin, F.; Kudritzki, R.P.; Storm, J.; et al. The Araucaria Project. A Distance Determination to the Local Group Spiral M33 from Near-infrared Photometry of Cepheid Variables. *Astrophys. J.* **2013**, *773*, 69. [CrossRef]
119. Scowcroft, V.; Freedman, W.L.; Madore, B.F.; Monson, A.J.; Persson, S.E.; Seibert, M.; Rigby, J.R.; Melbourne, J. The Carnegie Hubble Program: The Infrared Leavitt Law in IC 1613. *Astrophys. J.* **2013**, *773*, 106. [CrossRef]
120. Zinn, R.; Dahn, C.C. Variable 19 in NGC 5466: An anomalous cepheid in a globular cluster. *Astron. J.* **1976**, *81*, 527–533. [CrossRef]
121. Zinn, R.; Searle, L. The masses of the anomalous cepheids in the Draco system. *Astrophys. J.* **1976**, *209*, 734–747. [CrossRef]
122. Landi Dessy, J. Studies of Variables in the Magellanic Clouds: II. *Publ. Astron. Soc. Pac.* **1959**, *71*, 435. [CrossRef]
123. Plachy, E.; Szabó, R. RR Lyrae stars as seen by the Kepler space telescope. *Front. Astron. Space Sci.* **2021**, *7*, 81. [CrossRef]
124. Caputo, F.; Castellani, V.; Degl'Innocenti, S.; Fiorentino, G.; Marconi, M. Bright metal-poor variables: Why "Anomalous" Cepheids? *Astron. Astrophys.* **2004**, *424*, 927–934. [CrossRef]
125. Smith, H.A.; Stryker, L.L. Anomalous Cepheids in the Sculptor dwarf galaxy. *Astron. J.* **1986**, *92*, 328–334. [CrossRef]
126. Harris, H.C.; Silberman, N.A.; Smith, H.A. Variable Stars in the Draco Dwarf Spheroidal Galaxy. *A Half Century of Stellar Pulsation Interpretation*; Bradley, P.A., Guzik, J.A., Eds.; Astronomical Society of the Pacific Conference Series; 1998; Volume 135, p. 164. Available online: https://adsabs.harvard.edu/full/1996ASPC...92..536S (accessed on 24 October 2021).

127. Hoessel, J.G.; Saha, A.; Krist, J.; Danielson, G.E. Variable stars in the Leo A dwarf galaxy (DDO 69). *Astron. J.* **1994**, *108*, 645–652. [CrossRef]
128. Dolphin, A.E. Numerical methods of star formation history measurement and applications to seven dwarf spheroidals. *Mon. Not. R. Astron. Soc.* **2002**, *332*, 91–108. [CrossRef]
129. Fiorentino, G.; Stetson, P.B.; Monelli, M.; Bono, G.; Bernard, E.J.; Pietrinferni, A. On the Central Helium-burning Variable Stars of the LeoI Dwarf Spheroidal Galaxy. *Astrophys. J. Lett.* **2012**, *759*, L12. [CrossRef]
130. Norris, J.; Zinn, R. The cepheid variables and the stellar populations of the dwarf spheroidal galaxies. *Astrophys. J.* **1975**, *202*, 335–345. [CrossRef]
131. Renzini, A.; Mengel, J.G.; Sweigart, A.V. The anomalous Cepheids in dwarf spheroidal galaxies as binary systems. *Astron. Astrophys.* **1977**, *56*, 369–376.
132. Wheeler, J.C. Stars with anomalous mass—Is there funny business in the main sequence. *Comments Astrophys.* **1979**, *8*, 133–147.
133. Gautschy, A.; Saio, H. On binary channels to anomalous Cepheids. *Mon. Not. R. Astron. Soc.* **2017**, *468*, 4419–4428. [CrossRef]
134. Fiorentino, G.; Monelli, M. Anomalous Cepheids in the Large Magellanic Cloud. Insight into their origin and connection with the star formation history. *Astron. Astrophys.* **2012**, *540*, A102. [CrossRef]
135. Wallerstein, G. The Cepheids of Population II and Related Stars. *Publ. Astron. Soc. Pac.* **2002**, *114*, 689–699. [CrossRef]
136. Iwanek, P.; Soszyński, I.; Skowron, D.; Skowron, J.; Mróz, P.; Kozłowski, S.; Udalski, A.; Szymański, M.K.; Pietrukowicz, P.; Poleski, R.; et al. Three-Dimensional Distributions of Type II Cepheids and Anomalous Cepheids in the Magellanic Clouds. Do these Stars Belong to the Old, Young or Intermediate-Age Population? *Acta Astron.* **2018**, *68*, 213–236. [CrossRef]
137. Wallerstein, G.; Farrell, E.M. Kinematics of Type II Cepheids of the Galactic Halo. *Astron. J.* **2018**, *156*, 299. [CrossRef]
138. Prudil, Z.; Hanke, M.; Lemasle, B.; Crestani, J.; Braga, V.F.; Fabrizio, M.; Koch-Hansen, A.J.; Bono, G.; Grebel, E.K.; Matsunaga, N.; et al. Milky Way archaeology using RR Lyrae and type II Cepheids. I. The Orphan stream in 7D using RR Lyrae stars. *Astron. Astrophys.* **2021**, *648*, A78. [CrossRef]
139. Feast, M.W.; Laney, C.D.; Kinman, T.D.; van Leeuwen, F.; Whitelock, P.A. The luminosities and distance scales of type II Cepheid and RR Lyrae variables. *Mon. Not. R. Astron. Soc.* **2008**, *386*, 2115–2134. [CrossRef]
140. Matsunaga, N.; Feast, M.W.; Soszyński, I. Period-luminosity relations of type II Cepheids in the Magellanic Clouds. *Mon. Not. R. Astron. Soc.* **2011**, *413*, 223–234. [CrossRef]
141. Groenewegen, M.A.T.; Jurkovic, M.I. The period-luminosity and period-radius relations of Type II and anomalous Cepheids in the Large and Small Magellanic Clouds. *Astron. Astrophys.* **2017**, *604*, A29. [CrossRef]
142. Bhardwaj, A.; Macri, L.M.; Rejkuba, M.; Kanbur, S.M.; Ngeow, C.C.; Singh, H.P. Large Magellanic Cloud Near-infrared Synoptic Survey. IV. Leavitt Laws for Type II Cepheid Variables. *Astron. J.* **2017**, *153*, 154. [CrossRef]
143. Gingold, R.A. The evolutionary status of population II cepheids. *Astrophys. J.* **1976**, *204*, 116–130. [CrossRef]
144. Gingold, R.A. The evolutionary status of type II cepheids. *Mem. Della Soc. Astron. Ital.* **1985**, *56*, 169–192.
145. Di Criscienzo, M.; Caputo, F.; Marconi, M.; Cassisi, S. Synthetic properties of bright metal-poor variables. II. BL Hercules stars. *Astron. Astrophys.* **2007**, *471*, 893–900. [CrossRef]
146. Cox, J.P. Non-Adiabatic Stellar Pulsation. I. *Astrophys. J.* **1958**, *127*, 194. [CrossRef]
147. Zhevakin, S.A. On the Calculation of Nonadiabatic Stellar Pulsations by Use of a Discrete Model. *Astron. Zhurnal* **1959**, *36*, 269.
148. Cox, J.P. *Theory of Stellar Pulsation*; Princeton University Press: Princeton, NJ, USA, 1980.
149. Ritter, A. Untersuchungen über die Höhe der Atmosphäre und die Constitution gasförmiger Weltkörper. *Ann. Phys.* **1879**, *244*, 157–183. [CrossRef]
150. Bono, G.; Caputo, F.; Stellingwerf, R.F. On the Application of the Baade-Wesselink Method to RR Lyrae Stars. *Astrophys. J. Lett.* **1994**, *432*, L51. [CrossRef]
151. Stellingwerf, R.F. Convection in pulsating stars. I. Non linear hydro-dynamics. *Astrophys. J.* **1982**, *262*, 330–338. [CrossRef]
152. Bono, G.; Stellingwerf, R.F. Pulsation and Stability of RR Lyrae Stars. I. Instability Strip. *Astrophys. J.* **1994**, *93*, 233. [CrossRef]
153. Gehmeyr, M.; Winkler, K.H.A. On a new, one-dimensional, time-dependent model for turbulence and convection. I—A basic discussion of the mathematical model. II—An elementary comparison of the old and the new model. *Astron. Astrophys.* **1992**, *253*, 92–112.
154. Feuchtinger, M.U. A nonlinear convective model for radial stellar pulsations. I. The physical description. *Astron. Astrophys.* **1999**, *136*, 217–226. [CrossRef]
155. Szabó, R.; Kolláth, Z.; Buchler, J.R. Automated nonlinear stellar pulsation calculations: Applications to RR Lyrae stars. The slope of the fundamental blue edge and the first RRd model survey. *Astron. Astrophys.* **2004**, *425*, 627–639. [CrossRef]
156. van Albada, T.S.; Baker, N. On the Masses, Luminosities, and Compositions of Horizontal-Branch Stars. *Astrophys. J.* **1971**, *169*, 311. [CrossRef]
157. Bono, G.; Castellani, V.; Marconi, M. Classical Cepheid Pulsation Models. III. The Predictable Scenario. *Astrophys. J.* **2000**, *529*, 293–317. [CrossRef]
158. Di Criscienzo, M.; Caputo, F.; Marconi, M.; Musella, I. RR Lyrae-based calibration of the Globular Cluster Luminosity Function. *Mon. Not. R. Astron. Soc.* **2006**, *365*, 1357–1366. [CrossRef]
159. Marconi, M.; Fiorentino, G.; Caputo, F. Updated pulsation models for anomalous Cepheids. *Astron. Astrophys.* **2004**, *417*, 1101–1114. [CrossRef]

160. Fiorentino, G.; Limongi, M.; Caputo, F.; Marconi, M. Synthetic properties of bright metal-poor variables. I. "Anomalous" Cepheids. *Astron. Astrophys.* **2006**, *460*, 155–166. [CrossRef]
161. Bono, G.; Caputo, F.; Castellani, V.; Marconi, M.; Staiano, L.; Stellingwerf, R.F. The RR Lyrae fundamental red edge. *Astrophys. J.* **1995**, *442*, 159–162. [CrossRef]
162. Bono, G.; Caputo, F.; Stellingwerf, R.F. Synthetic Mean Colors for RR Lyrae Variables. *Astrophys. J.* **1995**, *99*, 263. [CrossRef]
163. Bono, G.; Caputo, F.; Marconi, M. The Topology of the RR Lyrae Instability Strip and the Oosterhoff Dichotomy. *Astron. J.* **1995**, *110*, 2365. [CrossRef]
164. Bono, G.; Caputo, F.; Cassisi, S.; Incerpi, R.; Marconi, M. Metal-rich RR Lyrae Variables. II. The Pulsational Scenario. *Astrophys. J.* **1997**, *483*, 811–825. [CrossRef]
165. Di Criscienzo, M.; Marconi, M.; Caputo, F. RR Lyrae Stars in Galactic Globular Clusters. III. Pulsational Predictions for Metal Content Z=0.0001 to Z=0.006. *Astrophys. J.* **2004**, *612*, 1092–1106. [CrossRef]
166. Marconi, M.; Minniti, D. Gauging the Helium Abundance of the Galactic Bulge RR Lyrae Stars. *Astrophys. J. Lett.* **2018**, *853*, L20. [CrossRef]
167. Bono, G.; Castellani, V.; Stellingwerf, R.F. Transient phenomena and modal stability in RR Lyrae and BL Herculis variable stars. *Astrophys. J. Lett.* **1995**, *445*, L145–L148. [CrossRef]
168. Bono, G.; Caputo, F.; Santolamazza, P.; Cassisi, S.; Piersimoni, A. Evolutionary Scenario for Metal-Poor Pulsating Stars. II. Anomalous Cepheids. *Astron. J.* **1997**, *113*, 2209. [CrossRef]
169. Bono, G.; Marconi, M. Cepheids in NGC 1866: A test for pulsational models. *Mon. Not. R. Astron. Soc.* **1997**, *290*, 353–359. [CrossRef]
170. Bono, G.; Caputo, F.; Castellani, V.; Marconi, M. Theoretical Models for Classical Cepheids. II. Period-Luminosity, Period-Color, and Period-Luminosity-Color Relations. *Astrophys. J.* **1999**, *512*, 711–723. [CrossRef]
171. Bono, G.; Marconi, M.; Stellingwerf, R.F. Classical Cepheid Pulsation Models. I. Physical Structure. *Astrophys. J.* **1999**, *122*, 167–205. [CrossRef]
172. Bono, G.; Castellani, V.; Marconi, M. The RR Lyrae Star U Comae as a Test for Nonlinear Pulsation Models. *Astrophys. J. Lett.* **2000**, *532*, L129–L132. [CrossRef]
173. Fiorentino, G.; Marconi, M.; Musella, I.; Caputo, F. Classical Cepheid pulsation models. XI. Effects of convection and chemical composition on the period-luminosity and period-Wesenheit relations. *Astron. Astrophys.* **2007**, *476*, 863–879. [CrossRef]
174. Marconi, M.; Musella, I.; Fiorentino, G.; Clementini, G.; Aloisi, A.; Annibali, F.; Contreras Ramos, R.; Saha, A.; Tosi, M.; van der Marel, R.P. Pulsation Models for Ultra-low (Z = 0.0004) Metallicity Classical Cepheids. *Astrophys. J.* **2010**, *713*, 615–625. [CrossRef]
175. Pietrzyński, G.; Graczyk, D.; Gieren, W.; Thompson, I.B.; Pilecki, B.; Udalski, A.; Soszyński, I.; Kozłowski, S.; Konorski, P.; Suchomska, K.; et al. An eclipsing-binary distance to the Large Magellanic Cloud accurate to two per cent. *New Astron.* **2013**, *495*, 76–79. [CrossRef]
176. Valle, G.; Marconi, M.; Degl'Innocenti, S.; Prada Moroni, P.G. Uncertainties on the theoretical predictions for classical Cepheid pulsational quantities. *Astron. Astrophys.* **2009**, *507*, 1541–1554. [CrossRef]
177. Marconi, M.; Degl'Innocenti, S. Modeling of RR Lyrae light curves: The case of M3. *Astron. Astrophys.* **2007**, *474*, 557–563. [CrossRef]
178. De Somma, G.; Marconi, M.; Molinaro, R.; Cignoni, M.; Musella, I.; Ripepi, V. An Extended Theoretical Scenario for Classical Cepheids. I. Modeling Galactic Cepheids in the Gaia Photometric System. *Astrophys. J.* **2020**, *247*, 30. [CrossRef]
179. De Somma, G.; Marconi, M.; Cassisi, S.; Ripepi, V.; Pietrinferni, A.; Molinaro, R.; Leccia, S.; Musella, I. Period-age-metallicity and period-age-colour-metallicity relations for classical Cepheids: An application to the Gaia EDR3 sample. *Mon. Not. R. Astron. Soc.* **2021**, *508*, 1473–1488. [CrossRef]
180. Fabrizio, M.; Braga, V.F.; Crestani, J.; Bono, G.; Ferraro, I.; Fiorentino, G.; Iannicola, G.; Preston, G.W.; Sneden, C.; Thévenin, F.; et al. On the Use of Field RR Lyrae As Galactic Probes: IV. New Insights Into and Around the Oosterhoff Dichotomy. *Astrophys. J.* **2021**, *919*, 118. [CrossRef]
181. Dolphin, A.E.; Saha, A.; Claver, J.; Skillman, E.D.; Cole, A.A.; Gallagher, J.S.; Tolstoy, E.; Dohm-Palmer, R.C.; Mateo, M. Variable Stars in Leo A: RR Lyrae Stars, Short-Period Cepheids, and Implications for Stellar Content. *Astron. J.* **2002**, *123*, 3154–3198. [CrossRef]
182. Glatt, K.; Gallagher, J.S., III.; Grebel, E.K.; Nota, A.; Sabbi, E.; Sirianni, M.; Clementini, G.; Tosi, M.; Harbeck, D.; Koch, A.; et al. An Accurate Age Determination for the Small Magellanic Cloud Star Cluster NGC 121 with the Hubble Space Telescope/Advanced Camera for Surveys. *Astron. J.* **2008**, *135*, 1106–1116. [CrossRef]
183. Venn, K.A.; Irwin, M.; Shetrone, M.D.; Tout, C.A.; Hill, V.; Tolstoy, E. Stellar Chemical Signatures and Hierarchical Galaxy Formation. *Astron. J.* **2004**, *128*, 1177–1195. [CrossRef]
184. Feltzing, S.; Chiba, M. Elemental abundances in the Milky Way stellar disk(s), bulge, and halo. *New Astron.* **2013**, *57*, 80–99. [CrossRef]
185. Fiorentino, G.; Bono, G.; Monelli, M.; Stetson, P.B.; Tolstoy, E.; Gallart, C.; Salaris, M.; Martínez-Vásquez, C.E.; Bernard, E.J. Weak Galactic Halo-Dwarf Spheroidal Connection from RR Lyrae Stars. *Astrophys. J. Lett.* **2015**, *798*, L12. [CrossRef]
186. Mayer, L. Environmental Mechanisms Shaping the Nature of Dwarf Spheroidal Galaxies: The View of Computer Simulations. *Adv. Astron.* **2010**, *2010*, 278434. [CrossRef]

187. Skillman, E.D.; Bender, R. *The Dwarf Galaxy Star Formation Crisis (Invited Paper)*; Pena, M., Kurtz, S., Eds.; Revista Mexicana de Astronomia y Astrofisica Conference Series; 1995; Volume 3, p. 25. Available online: https://adsabs.harvard.edu/full/1995RMxAC...3...25S (accessed on 17 November 2021).
188. Gallart, C.; Monelli, M.; Mayer, L.; Aparicio, A.; Battaglia, G.; Bernard, E.J.; Cassisi, S.; Cole, A.A.; Dolphin, A.E.; Drozdovsky, I.; et al. The ACS LCID Project: On the Origin of Dwarf Galaxy Types-A Manifestation of the Halo Assembly Bias? *Astrophys. J. Lett.* **2015**, *811*, L18. [CrossRef]
189. Fiorentino, G.; Monelli, M.; Stetson, P.B.; Bono, G.; Gallart, C.; Martínez-Vázquez, C.E.; Bernard, E.J.; Massari, D.; Braga, V.F.; Dall'Ora, M. Weak Galactic halo-Fornax dSph connection from RR Lyrae stars. *Astron. Astrophys.* **2017**, *599*, A125. [CrossRef]
190. Oosterhoff, P.T. Some remarks on the variable stars in globular clusters. *Observatory* **1939**, *62*, 104–109.
191. Fabrizio, M.; Bono, G.; Braga, V.F.; Magurno, D.; Marinoni, S.; Marrese, P.M.; Ferraro, I.; Fiorentino, G.; Giuffrida, G.; Iannicola, G.; et al. On the Use of Field RR Lyrae as Galactic Probes. I. The Oosterhoff Dichotomy Based on Fundamental Variables. *Astrophys. J.* **2019**, *882*, 169. [CrossRef]
192. Crestani, J.; Fabrizio, M.; Braga, V.F.; Sneden, C.; Preston, G.; Ferraro, I.; Iannicola, G.; Bono, G.; Alves-Brito, A.; Nonino, M.; et al. On the Use of Field RR Lyrae as Galactic Probes. II. A New ΔS Calibration to Estimate Their Metallicity. *Astrophys. J.* **2021**, *908*, 20. [CrossRef]
193. Crestani, J.; Braga, V.F.; Fabrizio, M.; Bono, G.; Sneden, C.; Preston, G.; Ferraro, I.; Iannicola, G.; Nonino, M.; Fiorentino, G.; et al. On the Use of Field RR Lyrae as Galactic Probes. III. The α-element Abundances. *Astrophys. J.* **2021**, *914*, 10. [CrossRef]
194. Gratton, R.; Sneden, C.; Carretta, E. Abundance Variations Within Globular Clusters. *Annu. Rev. Astron. Astrophys.* **2004**, *42*, 385–440. [CrossRef]
195. Borissova, J.; Minniti, D.; Rejkuba, M.; Alves, D.; Cook, K.H.; Freeman, K.C. Properties of RR Lyrae stars in the inner regions of the Large Magellanic Cloud. *Astron. Astrophys.* **2004**, *423*, 97–109. [CrossRef]
196. Borissova, J.; Minniti, D.; Rejkuba, M.; Alves, D. Properties of RR Lyrae stars in the inner regions of the Large Magellanic Cloud. II. The extended sample. *Astron. Astrophys.* **2006**, *460*, 459–466. [CrossRef]
197. Clementini, G.; Ripepi, V.; Bragaglia, A.; Martinez Fiorenzano, A.F.; Held, E.V.; Gratton, R.G. The metal abundance distribution of the oldest stellar component in the Sculptor dwarf spheroidal galaxy*. *Mon. Not. R. Astron. Soc.* **2005**, *363*, 734–748. [CrossRef]
198. Preston, G.W. A Spectroscopic Study of the RR Lyrae Stars. *Astrophys. J.* **1959**, *130*, 507. [CrossRef]
199. Jurcsik, J.; Kovacs, G. Determination of [Fe/H] from the light curves of RR Lyrae stars. *Astron. Astrophys.* **1996**, *312*, 111–120.
200. Alcock, C.; Allsman, R.A.; Alves, D.R.; Axelrod, T.S.; Basu, A.; Becker, A.C.; Bennett, D.P.; Cook, K.H.; Drake, A.J.; Freeman, K.C.; et al. The MACHO Project 9 Million Star Color-Magnitude Diagram of the Large Magellanic Cloud. *Astron. J.* **2000**, *119*, 2194–2213. [CrossRef]
201. Sarajedini, A.; Barker, M.K.; Geisler, D.; Harding, P.; Schommer, R. RR Lyrae Variables in M33. I. Evidence for a Field Halo Population. *Astron. J.* **2006**, *132*, 1361–1371. [CrossRef]
202. Pritzl, B.J.; Armandroff, T.E.; Jacoby, G.H.; Da Costa, G.S. The Dwarf Spheroidal Companions to M31: Variable Stars in Andromeda II. *Astron. J.* **2004**, *127*, 318–333. [CrossRef]
203. Sarajedini, A.; Barker, M.K.; Geisler, D.; Harding, P.; Schommer, R. Newly Identified Star Clusters in M33. I. Integrated Photometry and Color-Magnitude Diagrams. *Astron. J.* **2007**, *133*, 290–302. [CrossRef]
204. Braga, V.F.; Stetson, P.B.; Bono, G.; Dall'Ora, M.; Ferraro, I.; Fiorentino, G.; Freyhammer, L.M.; Iannicola, G.; Marengo, M.; Neeley, J.; et al. On the RR Lyrae Stars in Globulars. IV. ω Centauri Optical UBVRI Photometry. *Astron. J.* **2016**, *152*, 170. [CrossRef]
205. Martínez-Vázquez, C.E.; Monelli, M.; Bono, G.; Stetson, P.B.; Ferraro, I.; Bernard, E.J.; Gallart, C.; Fiorentino, G.; Iannicola, G.; Udalski, A. Variable stars in Local Group Galaxies—I. Tracing the early chemical enrichment and radial gradients in the Sculptor dSph with RR Lyrae stars. *Mon. Not. R. Astron. Soc.* **2015**, *454*, 1509–1516. [CrossRef]
206. Harbeck, D.; Grebel, E.K.; Holtzman, J.; Guhathakurta, P.; Brandner, W.; Geisler, D.; Sarajedini, A.; Dolphin, A.; Hurley-Keller, D.; Mateo, M. Population Gradients in Local Group Dwarf Spheroidal Galaxies. *Astron. J.* **2001**, *122*, 3092–3105. [CrossRef]
207. de Boer, T.J.L.; Tolstoy, E.; Hill, V.; Saha, A.; Olsen, K.; Starkenburg, E.; Lemasle, B.; Irwin, M.J.; Battaglia, G. The star formation and chemical evolution history of the sculptor dwarf spheroidal galaxyâ. *Astron. Astrophys.* **2012**, *539*, A103. [CrossRef]
208. Bernard, E.J.; Gallart, C.; Monelli, M.; Aparicio, A.; Cassisi, S.; Skillman, E.D.; Stetson, P.B.; Cole, A.A.; Drozdovsky, I.; Hidalgo, S.L.; et al. The ACS LCID Project: RR Lyrae Stars as Tracers of Old Population Gradients in the Isolated Dwarf Spheroidal Galaxy Tucana. *Astrophys. J. Lett.* **2008**, *678*, L21–L24. [CrossRef]
209. Mullen, J.P.; Marengo, M.; Martínez-Vázquez, C.E.; Neeley, J.R.; Bono, G.; Dall'Ora, M.; Chaboyer, B.; Thévenin, F.; Braga, V.F.; Crestani, J.; et al. Metallicity of Galactic RR Lyrae from Optical and Infrared Light Curves. I. Period-Fourier-Metallicity Relations for Fundamental-mode RR Lyrae. *Astrophys. J.* **2021**, *912*, 144. [CrossRef]
210. Sandage, A. Evidence for a period-luminosity-amplitude relation for RR Lyrae stars. *Astrophys. J. Lett.* **1981**, *244*, L23–L26. [CrossRef]
211. Sandage, A. The Oosterhoff period groups and the age of globular clusters. II. Properties of RR Lyrae stars in six clusters: The P-L-A relation. *Astrophys. J.* **1981**, *248*, 161–176. [CrossRef]
212. Walker, A.R. CCD observations of the RR Lyrae stars in NGC 2210 and the distance to the Large Magellanic Cloud. *Mon. Not. R. Astron. Soc.* **1985**, *212*, 343–352. [CrossRef]
213. Walker, A.R.; Mack, P. CCD Photometry of the RR Lyrae Stars in NGC 121 and the Distance to the Small Magellanic Cloud. *Astron. J.* **1988**, *96*, 872. [CrossRef]

214. Skowron, D.M.; Soszyński, I.; Udalski, A.; Szymański, M.K.; Pietrukowicz, P.; Skowron, J.; Poleski, R.; Wyrzykowski, Ł.; Ulaczyk, K.; Kozłowski, S.; et al. OGLE-ing the Magellanic System: Photometric Metallicity from Fundamental Mode RR Lyrae Stars. *Acta Astron.* **2016**, *66*, 269–292.
215. Bono, G. RR Lyrae Distance Scale: Theory and Observations. In *Stellar Candles for the Extragalactic Distance Scale*; Lecture Notes in Physics; Alloin, D., Gieren, W., Eds.; Springer: Berlin, Germany, 2003; Volume 635, pp. 85–104. [CrossRef]
216. Muraveva, T.; Delgado, H.E.; Clementini, G.; Sarro, L.M.; Garofalo, A. RR Lyrae stars as standard candles in the Gaia Data Release 2 Era. *Mon. Not. R. Astron. Soc.* **2018**, *481*, 1195–1211. [CrossRef]
217. Dambis, A.K.; Berdnikov, L.N.; Kniazev, A.Y.; Kravtsov, V.V.; Rastorguev, A.S.; Sefako, R.; Vozyakova, O.V. RR Lyrae variables: Visual and infrared luminosities, intrinsic colours and kinematics. *Mon. Not. R. Astron. Soc.* **2013**, *435*, 3206–3220. [CrossRef]
218. Chaboyer, B. Globular Cluster Distance Determinations. *Post-Hipparcos Cosm. Candles* **1999**, *237*, 111. [CrossRef]
219. Carretta, E.; Gratton, R.G.; Clementini, G. On the existence of differences in luminosity between horizontal branch stars in globular clusters and in the field. *Mon. Not. R. Astron. Soc.* **2000**, *316*, 721–728. [CrossRef]
220. Clementini, G.; Gratton, R.; Bragaglia, A.; Carretta, E.; Di Fabrizio, L.; Maio, M. Distance to the Large Magellanic Cloud: The RR Lyrae Stars. *Astron. J.* **2003**, *125*, 1309–1329. [CrossRef]
221. McNamara, D.H. The Absolute Magnitudes of the RR Lyrae Stars. *Publ. Astron. Soc. Pac.* **1997**, *109*, 857–867. [CrossRef]
222. Arenou, F.; Luri, X.; Babusiaux, C.; Fabricius, C.; Helmi, A.; Muraveva, T.; Robin, A.C.; Spoto, F.; Vallenari, A.; Antoja, T.; et al. Gaia Data Release 2. Catalogue validation. *Astron. Astrophys.* **2018**, *616*, A17. [CrossRef]
223. Cassisi, S.; Salaris, M. *Old Stellar Populations: How to Study the Fossil Record of Galaxy Formation*; Wiley: Hoboken, NJ, USA, 2013.
224. Nagarajan, P.; Weisz, D.R.; El-Badry, K. RR Lyrae-based Distances for 39 Nearby Dwarf Galaxies Calibrated to Gaia eDR3. *arXiv* **2021**, arXiv:2111.06899.
225. Longmore, A.J.; Fernley, J.A.; Jameson, R.F. RR Lyrae stars in globular clusters—Better distances from infrared measurements? *Mon. Not. R. Astron. Soc.* **1986**, *220*, 279–287. [CrossRef]
226. Bono, G.; Caputo, F.; Castellani, V.; Marconi, M.; Storm, J. Theoretical insights into the RR Lyrae K-band period-luminosity relation. *Mon. Not. R. Astron. Soc.* **2001**, *326*, 1183–1190. [CrossRef]
227. Bono, G.; Caputo, F.; Castellani, V.; Marconi, M.; Storm, J.; Degl'Innocenti, S. A pulsational approach to near-infrared and visual magnitudes of RR Lyr stars. *Mon. Not. R. Astron. Soc.* **2003**, *344*, 1097–1106. [CrossRef]
228. Madore, B.F.; Hoffman, D.; Freedman, W.L.; Kollmeier, J.A.; Monson, A.; Persson, S.E.; Rich, J.A., Jr.; Scowcroft, V.; Seibert, M. A Preliminary Calibration of the RR Lyrae Period-Luminosity Relation at Mid-infrared Wavelengths: WISE Data. *Astrophys. J.* **2013**, *776*, 135. [CrossRef]
229. Braga, V.F.; Stetson, P.B.; Bono, G.; Dall'Ora, M.; Ferraro, I.; Fiorentino, G.; Iannicola, G.; Inno, L.; Marengo, M.; Neeley, J.; et al. New near-infrared JHK$_s$ light-curve templates for RR Lyrae variables. *Astron. Astrophys.* **2019**, *625*, A1. [CrossRef]
230. Dall'Ora, M.; Storm, J.; Bono, G.; Ripepi, V.; Monelli, M.; Testa, V.; Andreuzzi, G.; Buonanno, R.; Caputo, F.; Castellani, V.; et al. The Distance to the Large Magellanic Cloud Cluster Reticulum from the K-Band Period-Luminosity-Metallicity Relation of RR Lyrae Stars. *Astrophys. J.* **2004**, *610*, 269–274. [CrossRef]
231. Sollima, A.; Cacciari, C.; Valenti, E. The RR Lyrae period-K-luminosity relation for globular clusters: An observational approach. *Mon. Not. R. Astron. Soc.* **2006**, *372*, 1675–1680. [CrossRef]
232. Muraveva, T.; Subramanian, S.; Clementini, G.; Cioni, M.R.L.; Palmer, M.; van Loon, J.T.; Moretti, M.I.; de Grijs, R.; Molinaro, R.; Ripepi, V.; et al. The VMC survey - XXVI. Structure of the Small Magellanic Cloud from RR Lyrae stars. *Mon. Not. R. Astron. Soc.* **2018**, *473*, 3131–3146. [CrossRef]
233. Pietrzyński, G.; Gieren, W.; Szewczyk, O.; Walker, A.; Rizzi, L.; Bresolin, F.; Kudritzki, R.P.; Nalewajko, K.; Storm, J.; Dall'Ora, M.; et al. The Araucaria Project: The Distance to the Sculptor Dwarf Spheroidal Galaxy from Infrared Photometry of RR Lyrae Stars. *Astron. J.* **2008**, *135*, 1993–1997. [CrossRef]
234. Szewczyk, O.; Pietrzyński, G.; Gieren, W.; Storm, J.; Walker, A.; Rizzi, L.; Kinemuchi, K.; Bresolin, F.; Kudritzki, R.P.; Dall'Ora, M. The Araucaria Project. The Distance of the Large Magellanic Cloud from Near-Infrared Photometry of RR Lyrae Variables. *Astron. J.* **2008**, *136*, 272–279. [CrossRef]
235. Szewczyk, O.; Pietrzyński, G.; Gieren, W.; Ciechanowska, A.; Bresolin, F.; Kudritzki, R.P. The Araucaria Project: The Distance to the Small Magellanic Cloud from Near-Infrared Photometry of RR Lyrae Variables. *Astron. J.* **2009**, *138*, 1661–1666. [CrossRef]
236. Karczmarek, P.; Pietrzyński, G.; Gieren, W.; Suchomska, K.; Konorski, P.; Górski, M.; Pilecki, B.; Graczyk, D.; Wielgórski, P. The Araucaria Project: The Distance to the Carina Dwarf Galaxy from Infrared Photometry of RR Lyrae Stars. *Astron. J.* **2015**, *150*, 90. [CrossRef]
237. Karczmarek, P.; Pietrzyński, G.; Górski, M.; Gieren, W.; Bersier, D. The Araucaria Project: The Distance to the Fornax Dwarf Galaxy from Near-infrared Photometry of RR Lyrae Stars. *Astron. J.* **2017**, *154*, 263. [CrossRef]
238. Hatt, D.; Beaton, R.L.; Freedman, W.L.; Madore, B.F.; Jang, I.S.; Hoyt, T.J.; Lee, M.G.; Monson, A.J.; Rich, J.A.; Scowcroft, V.; et al. The Carnegie-Chicago Hubble Program. II. The Distance to IC 1613: The Tip of the Red Giant Branch and RR Lyrae Period-luminosity Relations. *Astrophys. J.* **2017**, *845*, 146. [CrossRef]
239. Dékány, I.; Minniti, D.; Catelan, M.; Zoccali, M.; Saito, R.K.; Hempel, M.; Gonzalez, O.A. VVV Survey Near-infrared Photometry of Known Bulge RR Lyrae Stars: The Distance to the Galactic Center and Absence of a Barred Distribution of the Metal-poor Population. *Astrophys. J. Lett.* **2013**, *776*, L19. [CrossRef]

240. Contreras Ramos, R.; Minniti, D.; Gran, F.; Zoccali, M.; Alonso-García, J.; Huijse, P.; Navarro, M.G.; Rojas-Arriagada, Á.; Valenti, E. The VVV Survey RR Lyrae Population in the Galactic Center Region. *Astrophys. J.* **2018**, *863*, 79. [CrossRef]
241. Muraveva, T.; Garofalo, A.; Scowcroft, V.; Clementini, G.; Freedman, W.L.; Madore, B.F.; Monson, A.J. The Carnegie RR Lyrae Program: Mid-infrared period-luminosity relations of RR Lyrae stars in Reticulum. *Mon. Not. R. Astron. Soc.* **2018**, *480*, 4138–4153. [CrossRef]
242. Cusano, F.; Moretti, M.I.; Clementini, G.; Ripepi, V.; Marconi, M.; Cioni, M.R.L.; Rubele, S.; Garofalo, A.; de Grijs, R.; Groenewegen, M.A.T.; et al. The VMC Survey—XLII. Near-infrared period-luminosity relations for RR Lyrae stars and the structure of the Large Magellanic Cloud. *Mon. Not. R. Astron. Soc.* **2021**, *504*, 1–15. [CrossRef]
243. Marconi, M.; Bono, G.; Pietrinferni, A.; Braga, V.F.; Castellani, M.; Stellingwerf, R.F. On the Impact of Helium Content on the RR Lyrae Distance Scale. *Astrophys. J. Lett.* **2018**, *864*, L13. [CrossRef]
244. Bhardwaj, A. High-precision distance measurements with classical pulsating stars. *J. Astrophys. Astron.* **2020**, *41*, 23. [CrossRef]
245. Marconi, M.; Molinaro, R.; Ripepi, V.; Leccia, S.; Musella, I.; De Somma, G.; Gatto, M.; Moretti, M.I. A theoretical scenario for Galactic RR Lyrae in the Gaia data base: Constraints on the parallax offset. *Mon. Not. R. Astron. Soc.* **2021**, *500*, 5009–5023. [CrossRef]
246. Christy, R.F. Lectures on Variable Stars (concluded). *J. R. Astron. Soc. Can.* **1970**, *64*, 8.
247. Demarque, P.; Hirshfeld, A.W. On the nature of the bright variables in dwarf spheroidal galaxies. *Astrophys. J.* **1975**, *202*, 346–352. [CrossRef]
248. Castellani, V.; degl'Innocenti, S. Dwarf spheroidals and the evolution of not-too-old Population II stars. *Astron. Astrophys.* **1995**, *298*, 827.
249. Caputo, F.; Cassisi, S.; Castellani, M.; Marconi, G.; Santolamazza, P. Stellar Populations in the Dwarf Spheroidal Galaxy Leo I. *Astron. J.* **1999**, *117*, 2199–2210. [CrossRef]
250. Sills, A.; Karakas, A.; Lattanzio, J. Blue Stragglers After the Main Sequence. *Astrophys. J.* **2009**, *692*, 1411–1420. [CrossRef]
251. Gallart, C.; Bernard, E.J.; Brook, C.B.; Ruiz-Lara, T.; Cassisi, S.; Hill, V.; Monelli, M. Uncovering the birth of the Milky Way through accurate stellar ages with Gaia. *Nat. Astron.* **2019**, *3*, 932–939. [CrossRef]
252. Fiorentino, G.; Marconi, M.; Bono, G.; Dalessandro, E.; Ferraro, F.R.; Lanzoni, B.; Lovisi, L.; Mucciarelli, A. Blue Straggler Masses from Pulsation Properties. II. Topology of the Instability Strip. *Astrophys. J.* **2015**, *810*, 15. [CrossRef]
253. Richards, J.W.; Starr, D.L.; Butler, N.R.; Bloom, J.S.; Brewer, J.M.; Crellin-Quick, A.; Higgins, J.; Kennedy, R.; Rischard, M. On Machine-learned Classification of Variable Stars with Sparse and Noisy Time-series Data. *Astrophys. J.* **2011**, *733*, 10. [CrossRef]
254. Elorrieta, F.; Eyheramendy, S.; Jordán, A.; Dékány, I.; Catelan, M.; Angeloni, R.; Alonso-García, J.; Contreras-Ramos, R.; Gran, F.; Hajdu, G.; et al. A machine learned classifier for RR Lyrae in the VVV survey. *Astron. Astrophys.* **2016**, *595*, A82. [CrossRef]
255. Hernitschek, N.; Schlafly, E.F.; Sesar, B.; Rix, H.W.; Hogg, D.W.; Ivezić, Ž.; Grebel, E.K.; Bell, E.F.; Martin, N.F.; Burgett, W.S.; et al. Finding, Characterizing, and Classifying Variable Sources in Multi-epoch Sky Surveys: QSOs and RR Lyrae in PS1 3π data. *Astrophys. J.* **2016**, *817*, 73. [CrossRef]
256. Holl, B.; Audard, M.; Nienartowicz, K.; Jevardat de Fombelle, G.; Marchal, O.; Mowlavi, N.; Clementini, G.; De Ridder, J.; Evans, D.W.; Guy, L.P.; et al. Gaia Data Release 2. Summary of the variability processing and analysis results. *Astron. Astrophys.* **2018**, *618*, A30. [CrossRef]
257. Hosenie, Z.; Lyon, R.J.; Stappers, B.W.; Mootoovaloo, A. Comparing Multiclass, Binary, and Hierarchical Machine Learning Classification schemes for variable stars. *Mon. Not. R. Astron. Soc.* **2019**, *488*, 4858–4872. [CrossRef]
258. Massari, D.; Koppelman, H.H.; Helmi, A. Origin of the system of globular clusters in the Milky Way. *Astron. Astrophys.* **2019**, *630*, L4. [CrossRef]
259. McConnachie, A.W.; Irwin, M.J.; Ibata, R.A.; Dubinski, J.; Widrow, L.M.; Martin, N.F.; Côté, P.; Dotter, A.L.; Navarro, J.F.; Ferguson, A.M.N.; et al. The remnants of galaxy formation from a panoramic survey of the region around M31. *New Astron.* **2009**, *461*, 66–69. [CrossRef] [PubMed]
260. Stetson, P.B. Homogeneous Photometry for Star Clusters and Resolved Galaxies. II. Photometric Standard Stars. *Publ. Astron. Soc. Pac.* **2000**, *112*, 925–931. [CrossRef]
261. Dall'Ora, M.; Clementini, G.; Kinemuchi, K.; Ripepi, V.; Marconi, M.; Di Fabrizio, L.; Greco, C.; Rodgers, C.T.; Kuehn, C.; Smith, H.A. Variable Stars in the Newly Discovered Milky Way Satellite in Bootes. *Astrophys. J. Lett.* **2006**, *653*, L109–L112. [CrossRef]
262. Clementini, G.; Cignoni, M.; Contreras Ramos, R.; Federici, L.; Ripepi, V.; Marconi, M.; Tosi, M.; Musella, I. Variability and Star Formation in Leo T, the Lowest Luminosity Star-forming Galaxy Known Today. *Astrophys. J.* **2012**, *756*, 108. [CrossRef]
263. Saha, A.; Hoessel, J.G. RR Lyrae stars in local group galaxies. I—NGC 185. *Astron. J.* **1990**, *99*, 97–148. [CrossRef]
264. Saha, A.; Hoessel, J.G.; Mossman, A.E. RR Lyrae stars in local group galaxies. II—NGC 147. *Astron. J.* **1990**, *100*, 108–126. [CrossRef]
265. Pritzl, B.J.; Armandroff, T.E.; Jacoby, G.H.; Da Costa, G.S. The Dwarf Spheroidal Companions to M31: Variable Stars in Andromeda I and Andromeda III. *Astron. J.* **2005**, *129*, 2232–2256. [CrossRef]